CHARACTERIZATION OF VANADIUM OXIDE THIN FILMS GROWN BY MAGNETRON SPUTTERING TECHNIQUE

A Thesis Submitted to
the Graduate School of Engineering and Sciences of
İzmir Institute of Technology
in Partial Fulfillment of the Requirements for the Degree of

MASTER OF SCIENCE

in Physics

by
Hürriyet YÜCE

October 2015
İZMİR

We approve the thesis of **Hürriyet YÜCE**

Examining Committee Members:

____

Prof. Dr. Lütfi ÖZYÜZER
Department of Physics, İzmir Institute of Technology

____

Prof. Dr. Serhan ÖZDEMİR
Department of Mechanical Engineering, İzmir Institute of Technology

____

Prof. Dr. Talat YALÇIN
Department of Chemistry, İzmir Institute of Technology

____

Assoc. Prof. Dr. Ekrem ÖZDEMİR
Department of Chemical Engineering, İzmir Institute of Technology

____

Asst. Prof. Dr. Mehtap ÖZDEMİR KÖKLÜ
Department of Electrical-Electronics Engineering, Gediz University

27 October 2015

____

Prof. Dr. Lütfi ÖZYÜZER
Supervisor, Department of Physics
İzmir Institute of Technology

____

Prof. Dr. Nejat BULUT
Head of the Department of Physics

____

Prof. Dr. Bilge KARAÇALI
Dean of the Graduated School of
Engineering and Science

ACKNOWLEDGEMENTS

Firstly and above all, I would like to express the deepest gratitude to my advisor Prof. Dr. Lütfi ÖZYÜZER for his guidance and support during my master thesis studies. I also would like to thank my project director Assoc. Prof. Dr. Gülnur AYGÜN ÖZYÜZER who supported and motivated me during my research.

I would like thank also the members of my thesis defense committee Prof. Dr. Serhan ÖZDEMİR, Prof. Dr. Talat YALÇIN, Assoc. Prof. Dr. Ekrem ÖZDEMİR and Asst. Prof. Dr. Mehtap ÖZDEMİR KÖKLÜ for their useful comments and suggestions.

Special thanks to my all group members for their help and creating a friendly and productive environment. Their remarkable outlook obligated me come up with new research ideas.

I wish to express my cordial appreciation to my family for their consistent support and love during my education. I am exceptionally fortunate to be blessed with a perfect family.

Finally, I would like to thank TÜBİTAK for supporting the project 113F349 which has been supervised by Assoc. Prof. Dr. Gülnur AYGÜN ÖZYÜZER during my thesis.

ABSTRACT

CHARACTERIZATION OF VANADIUM OXIDE THIN FILMS GROWN BY MAGNETRON SPUTTERING TECHNIQUE

Vanadium dioxide (VO_2) exhibits metal insulator transition (MIT) at around 70 °C. VO_2 shows insulator phase at low temperature whereas above the transition temperature VO_2 shows metallic phase. The resistivity of this material abruptly changes by a factor of 10^4 at MIT temperature. There are some factors which induce MIT in VO_2 structure such as electric field, the change in temperature or doping. Due to these properties, VO_2 is an interesting candidate for exploring potential applications in high speed electronic devices. VO_2 plays an important role for field effect transistor (FET) applications. VO_2 with its peculiar properties is a good candidate for channel material in FET. Electric field triggered MIT is a desired feature for FET applications.

In this work, VO_2 thin films have been deposited on c-cut sapphire [Al_2O_3(0001)] substrate by using DC magnetron sputtering technique. In order to obtain the homogeneous VO_2 thin film, the growth process was carried out at various oxygen flow rates with different deposition time. To obtain single VO_2 phase, optimum oxygen rate was investigated with various analysis techniques such as Raman, X-ray diffraction (XRD) and X-ray photoelectron spectroscopy (XPS) and optical-electrical measurements. At the same time, the temperature dependences of optical-electrical properties of these films were analyzed. Then, the metal insulator transition was observed with the change in resistivity by a factor of 10^4 which is the highest value among grown VO_2 films by sputtering technique in the literature.

For FET applications, the grown VO_2 thin film which indicates the highest change in resistivity at transition temperature was patterned by electron beam lithography in order to create FET channel schema. After electron beam lithography process, the electrical properties of the VO_2 strips with various widths were analyzed. The effects of the widths of the VO_2 strips on their electrical properties were investigated.

ÖZET

MIKNATISSAL SAÇTIRMA YÖNTEMİ İLE BÜYÜTÜLEN VANADYUM OKSİT İNCE FİLMLERİN KARAKTERİZASYONU

Vanadyum dioksit (VO_2) yaklaşık olarak 70 °C'de metal-yalıtkan geçiş özelliği göstermektedir. VO_2 düşük sıcaklıklarda yalıtkan fazda bulunurken, geçiş sıcaklığına göre yüksek sıcaklıklarda metalik fazda bulunur. Geçiş sıcaklığında, VO_2'nin özdirenci ani bir şekilde 10^4 oranında değişim gösterir ve bu özelliğinden dolayı hızlı elektronik cihazlarda kullanılma potansiyeli oldukça yüksektir. VO_2 alan etkili transistör uygulamalarında önemli bir rol oynamaktadır. VO_2 gösterdiği elektriksel özellikler sebebiyle alan etkili transistörlerde kanal görevi görmektedir. VO_2 malzemesinin elektrik alan altında değişen elektriksel özellikleri, VO_2'yi alan etkili transistörlerde kanal malzemesi olarak kullanılmasını mümkün kılmaktadır.

Bu çalışmada DC mıknatıssal saçtırma tekniği kullanarak, VO_2 c-düzlem safir [Al_2O_3(0001)] alttaş üzerine büyütülmüştür. Büyütülen ince filmlerde homojen VO_2 yapısı elde edebilmek için, VO_2 büyütme parametreleri farklı oksijen akış oranlarında ve farklı biriktirme sürelerinde değişiklik göstermektedir. Tek fazda VO_2 elde edebilmek için, Raman, X ışınları saçılımı (XRD) ve X-ışını fotoelektron spektroskopisi (XPS) gibi çeşitli analiz teknikleri kullanılmış olup, optiksel-elektriksel analiz sonuçlarına göre en uygun oksijen oranı araştırılmıştır. Aynı zamanda, VO_2 ince filmlerin optiksel-elektriksel özellikleri sıcaklığa bağlı olarak ayrıca analiz edilmiştir. Geçiş sıcaklığında 10^4 oranında değişen bir özdirenç değeriyle, literatürdeki mıknatıssal saçtırma yöntemi ile elde edilen en iyi sonuçtur.

Büyütülen vanadyum oksit ince filmleri arasında metal-yalıtkan geçiş sıcaklığında en yüksek özdirenç değişimi gösteren VO_2 ince film, alan etkili transistor uygulamaları açısından kanal görevi görecek olması sebebiyle, elektron demeti litografisiyle kanal şekli verilerek şekillendirilmiştir. Elektron demeti litografi süreci sonrasında, farklı genişliklerdeki VO_2 şeritlerinin elektriksel özellikleri incelenmiş olup, VO_2 şeritlerinin genişliğinin elektriksel özelliği üzerindeki etkileri tartışılmıştır.

To My Dear Family

TABLE OF CONTENTS

LIST OF FIGURES ... x

LIST OF TABLES ... xii

CHAPTER 1. INTRODUCTION ... 1

1.1. Introduction and Motivation ... 1

1.2. Vanadium Dioxide (VO_2): A Review ... 2

1.2.1. Crystal structure of VO_2 ... 4

1.2.2. Electronic Properties of VO_2 ... 5

1.2.3. Phase Diagram in VO_2 Structure ... 6

1.2.4. Phase Transition in VO_2 ... 7

1.2.4.1. Mott-Hubbard Transition ... 7

1.2.4.2. Peierls Transition ... 12

1.3. The Applications of VO_2 ... 13

1.3.1. Multifunctional Artificial Muscles ... 13

1.3.2. Thermochromic Smart Windows ... 13

1.3.3. Infrared Detectors ... 14

1.3.4. Field Effect Transistors (FET) ... 16

1.4. Contents of This Dissertation ... 16

CHAPTER 2. THIN FILM GROWTH PROCESSING ... 18

2.1. Thin Film Growth ... 18

2.2. Sputtering Method ... 19

2.3. Plasma ... 20

2.4. Atomic Collisions ... 21

2.5. Nucleation and Growth ... 22

2.6. Deposition on Sample 23

2.7. The Mean Free Path 24

2.8. Sputter Yield 24

2.9. Sputtering Systems 25

2.9.1. Direct Current (DC) Sputtering 25

2.9.2. Radio Frequency (RF) Sputtering 26

2.9.3. Reactive Sputtering 27

2.9.4. Magnetron Sputtering 27

CHAPTER 3. EXPERIMENTAL PROCEDURE 29

3.1. Purpose 29

3.2. Experimental Process for Vanadium Oxide Thin Films on c-cut Sapphire [Al_2O_3 (0001)] 29

3.3. Vanadium Oxide Thin Film Fabrication Method 31

3.3.1. Magnetron Sputtering System 31

3.4. Measurement Systems 32

3.4.1. Scanning Electron Microscopy (SEM) 32

3.4.2. X-ray Diffraction (XRD) 32

3.4.3. Raman Spectroscopy 33

3.4.4. X-Ray Photoelectron Spectroscopy (XPS) 34

3.4.5. Optical Characterization 35

3.4.6. Electrical Characterization 35

3.5. E-Beam Lithography Process of Shaped VO_2 Films 36

3.5.1 Clean Room Process 36

3.5.2. Electron-Beam Lithography 37

3.5.3. Ion Beam Etching 38

CHAPTER 4. RESULTS AND DISCUSSIONS 41

4.1. Scanning Electron Microscopy (SEM) Morphological Analysis 41
4.2. X-Ray Diffraction (XRD) Analysis 42
4.3. Raman Analysis 45
4.4. Optical Properties 47
4.5. X-Ray Photoelectron Spectroscopy (XPS) Analysis 50
4.6. Electrical Properties 52

CHAPTER 5. CONCLUSION 55

REFERENCES 57

LIST OF FIGURES

Figure **Page**

Figure 1.1. The graph of the MIT in VO_2 by (a) heating (b) UV light (c) Electric field..........3
Figure 1.2. The crystallographic structure of (a) VO_2 (M); (b) VO_2 (R)..........4
Figure 1.3. The electronic band structure of metallic and insulator VO_2..........5
Figure 1.4. Strain-temperature phase diagram of VO_2 material..........7
Figure 1.5. Two different electronic configurations in 2-Dimensional crystal it has (a) lower (b) higher energy because of Coulomb repulsion..........8
Figure 1.6. The schema of 1-Dimensional chain with one electron per unit cell with lower and upper band..........9
Figure 1.7. (a) A reverse transformation from k-space to real-space for an inhomogeneous system (b) when averaged over lattice, the state of being of homogeneous system from inhomogeneous system..........11
Figure 1.8. (a) The curve of the effective mass of quasi-particle (b) Mott insulator-metal with hole doping..........12
Figure 1.9. Schematic description of Peierls metal-insulator transition in a linear chain..........13
Figure 1.10. VO_2-based smart windows..........14
Figure 1.11. TCR measurement scheme..........15
Figure 1.12. A diagram of field effect transistor (FET) device..........16
Figure 2.1. Sputtering schema..........20
Figure 2.2. The image of the various thin film growth modes..........23
Figure 2.3. The basic system of the DC sputtering..........26
Figure 2.4. Basic elements of RF sputtering..........27
Figure 3.1. The picture of (a) magnetron sputtering system (b) growth chamber..........31
Figure 3.2. X-ray diffraction pattern..........33
Figure 3.3. The picture of probe station..........36
Figure 3.4. Schematic presentation of clean room and electron beam..........37
Figure 3.5. Electron beam lithography system..........38
Figure 3.6. Schematic image of ion beam etching system..........39
Figure 3.7. VO_2 strips with various widths..........40

Figure 4.1. Schematic representation of VO_2 thin films on c-cut sapphire substrate with different thickness and oxygen concentration 42
Figure 4.2. FE-SEM images of (a) 310 nm VO_2 thin film with 2.00 % oxygen ratio (b) 125 nm VO_2 thin film with 2.25 % oxygen ratio 42
Figure 4.3. XRD pattern of 310 nm VO_2 thin film with 2.00 % oxygen ratio 44
Figure 4.4. XRD pattern of 125 nm VO_2 thin film with 2.25 % oxygen ratio................ 45
Figure 4.5. Raman spectra of grown VO_2 thin films with the thickness of 125 and 310 nm at various oxygen ratio.. 47
Figure 4.6. Transmittance spectra of 310 nm grown VO_2 thin film with 2.00 % oxygen ratio at room temperature and 80 ^{o}C 48
Figure 4.7. Transmittance spectra of 125 nm grown VO_2 thin films with various oxygen ratio at room temperature and 80 ^{o}C 49
Figure 4.8. Optical switching property depends on the temperature of 125 nm VO_2 thin film with 2.25 % oxygen ratio as different wavelength........................ 50
Figure 4.9. XPS analysis of carbon (C) 51
Figure 4.10. XPS analysis of 310 nm VO_2 thin film with 2.00 % concentration 52
Figure 4.11. The resistivity depends on the temperature for 310 nm VO_2 thin film with 2.00 % oxygen ratio and 125 nm VO_2 thin films with 2.25 % oxygen ratio 53
Figure 4.12. The resistivity depends on the temperature for shaped 310 nm VO_2 thin film at 2.00 % oxygen ratio. 54

LIST OF TABLES

Table **Page**

Table 1.1. Selected data of VO_x compounds depends on oxygen content. The third row shows transition temperatures of the materials. 2

CHAPTER 1

INTRODUCTION

1.1. Introduction and Motivation

Metal-Oxide Semiconductor field effect transistor (MOSFET) has been an important element of electronic industry for a long while. The size of MOSFET has been reducing for a long time in compliance with Moore's Law. At the present time, as the size of MOSFET is made smaller, some complications emerge due to main limitations such as quantum mechanical electron tunneling and sophisticated fabrication techniques. Alternative processes and techniques are currently designed in order to improve integration and to develop the performance of electronic systems. Metal-oxide electronics is one of the promising approaches for developing electronic systems.

Strongly interacting d-orbital electrons in transition metal oxides leads to strong electron-electron correlations. This behavior is important for the mechanism of metal-insulator transition (MIT). Electric field dependence of MIT is a promising mechanism for fabricating field effect transistors (FETs) based on the metal-insulator transition (Belyaev et al. 2014).

A first order phase transition, which describes the transition between two dissimilar phases of a material at a specific temperature, conventionally takes place by a change in a field variable such as pressure, temperature, magnetic or electrical field. As a phase transition includes collective phenomena, resolving microscopic process at work can be difficult. The metal-insulator transition is such a transition with its quantum nature and with a sudden state change between metallic and conducting phase. One of the best known materials which have MIT property is VO_2.

All of vanadium oxide compounds have strong electron-electron correlation and show MIT except V_7O_{13} material (Wu, Feng, and Xie 2013). Among vanadium oxide (VO_x) compounds, VO_2 exhibits the phase transition at around 70 ℃ which is the nearest transition temperature to room temperature compared to the transition temperatures of the other vanadium oxide compounds (Stefanovich, Pergament, and Stefanovich 2000, Gopalakrishnan, Ruzmetov, and Ramanathan 2009). At the same

time, not only electric field (Ruzmetov et al. 2009) also heating (Yuce et al. 2015) across over transition temperature induces MIT. The change in the resistivity of VO_2 is by a factor of 10^4-10^5 during MIT (Chae et al. 2003). Because of this property which is high change in resistivity, VO_2 has high potential for future technological devices. The purpose of this work is to fabricate VO_2 channel in order to utilize the MIT in VO_2 structure under electric field for FET applications.

1.2. Vanadium Dioxide (VO_2): A Review

Since VO_2 material was discovered by F. J. Morin in the 1950s, vanadium oxides compounds have been extensively studied. Vanadium dioxide (VO_2) is a particularly important material because of the fact that MIT in this material takes place closest to room temperature compared to the other vanadium oxide compounds. The oxygen content in these compounds plays a large role at the transition temperature. The temperatures are given in Table 1.1 with their oxygen contents at the second row.

Table 1.1. Selected data of VO_x compounds depends on oxygen content. The third row shows transition temperatures of the materials.

Material	VO	V_2O_3	V_7O_{13}	VO_2	V_6O_{13}	V_2O_5
x (VO_x)	1.00	1.50	1.85	2.00	2.16	2.50
T_{MIT}	-147 ºC (Johansson 2006)]	-105 ºC (Wu, Feng, and Xie 2013)	-	70 ºC (Jordan et al. 2014)	-123 ºC (Eguchi et al. 2002)	375 ºC (Filonenko et al. 2004)

The MIT in VO_2 has been a focus of intense experimental and theoretical research due to the 4-5 order of magnitude change in resistivity at 70 ˚C MIT temperature (T_{MIT}) (Figure 1.1a), the closeness of this transition to room temperature and fast MIT switching upon optical excitation properties. A drop in the resistivity of VO_2 is observed at transition temperature, and low temperature VO_2 indicates insulator phase whereas this material indicates metallic phase at higher temperature than T_{MIT}. In addition to heating, there are various external factors such as doping (Tan et al. 2012)

UV light (Wu and Liou 2011) or electric field (Kim et al. 2004) in order to induce MIT in VO_2. As shown in Figure 1.1b, VO_2 with 0.65 eV band gap is exposed to UV light. Under UV light, photoexcited carriers generate in conduction band of VO_2, and VO_2 becomes a metal with increasing carrier density. Additionally, under electric field, charge accumulation occurs, and MIT takes place with increasing electron/hole density (Figure 1.1c).

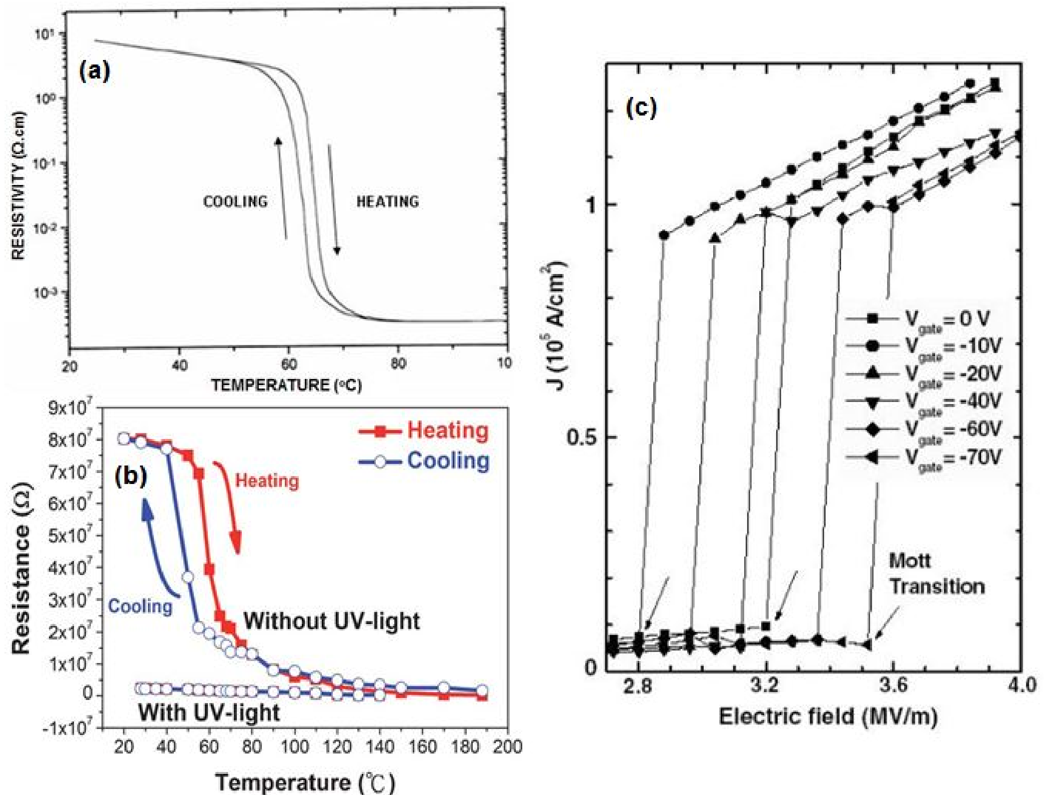

Figure 1.1. The graph of the MIT in VO_2 by (a) heating (b) UV light (c) Electric field (Source: Nag 2011, Wu and Liou 2011, Kim et al. 2004)

There are two different mechanisms which are responsible for MIT; first one is Mott-Hubbard transition and the other one is Peierls transition. According to Peierls transition, above MIT temperature, the crystal structure changes. Then, the band gap vanishes and VO_2 becomes a metal. This view can be explained by the single electron picture. The other view is Mott-Hubbard transition. In the Mott insulator, although Fermi energy level crosses the conduction band, the structure still shows an insulator phase. Furthermore, this is clue to electron correlation effects. By changing the temperature, a phase transition takes place. In addition, ordinary band theory cannot

explain this phenomenon. As considering these two views, there is no clear answer yet (Imada, Fujimori, and Tokura 1998, Basov et al. 2011).

1.2.1. Crystal structure of VO_2

VO_2 has two different crystal structures with electronically its different states. While VO_2 shows insulator phase with monoclinic crystal structure at low temperature, this material indicates metallic phase with tetragonal rutile crystal structure at high temperature. The crystal structure is shown in Figure 1.2 where oxygen atom is shown in red color and vanadium in grey color. There are two possible values of V-V distances. The distance between the nearest V-V dimers is 0.262 nm, and the distance for zigzag-type V atom chains along the c_R-axis is 0.316 nm. The distance of critical V-V interaction is 0.294 nm (Ohno 1998). In this situation, V-V distance (0.316 nm) is larger than critical V-V interaction distances, d-orbital electrons inside the dimers are localized, which exhibits insulating behavior of VO_2 (M), with resistivity of around 10 Ω.cm. For metallic VO_2(R), when the average distance of V-V atoms is 0.288 nm, all of vanadium ions are aligned in one line. Thus, all metal V atoms have overlapping d-orbital electrons, which leads to metallic behavior of VO_2 (R), with a resistivity of nearly 10^{-4} Ω.cm (Wu, Feng, and Xie 2013).

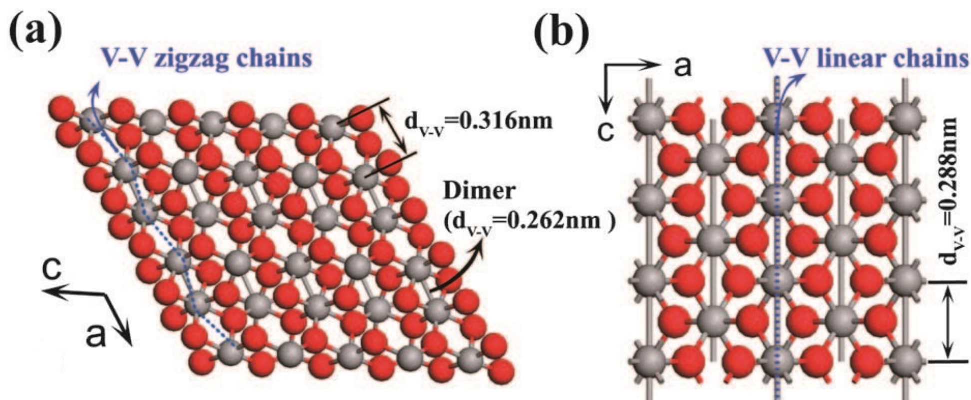

Figure 1.2. The crystallographic structure of (a) VO_2 (M); (b) VO_2 (R)
(Source: Wu, Feng, and Xie 2013)

1.2.2. Electronic Properties of VO_2

The figure of the electronic band structures of metallic and insulator VO_2 which is compatible Goodenough's model is shown in Figure 1.3. The band structure of VO_2 is formed with O_{2p} and V_{3d} orbitals, and contains π and σ bonds of 2p orbital. Each vanadium (V) atoms in VO_2 structure has one d-orbital e^-.

For tetragonal crystal structure of VO_2, t_{2g} levels in the crystal are split into d_{ll} and π^* levels which include the electronic states near Fermi energy level for metallic phase. The dıı orbitals are hybridized with each other forming the valence band. On the other hand, $d_{3z^2-r^2}$ orbitals hybridized with O_{2p} orbital. For d-orbitals in V cations, degenerated t_{2g} states are $d_{x^2-y^2}$, d_{xz} and d_{yz} and the other one is e_g^σ (σ antibonding, σ^*) orbitals which are $d_{3z^2-r^2}$ and d_{xy}. When the crystal structure changes from monoclinic to tetragonal, the π^* energy level becomes higher than the energy level of d_{ll} (Nazari 2013).

For monoclinic crystal structure of VO_2, d_{ll} bands are separated into lower and upper bands in the event of the pairing of V atoms along the c_R direction. V-V pairing increases vanadium d-orbital and oxygen p-orbital hybridization. Moreover, this pairing increases π^* energy level above the Fermi level, and this causes 0.65 eV band gap (Imada, Fujimori, and Tokura 1998).

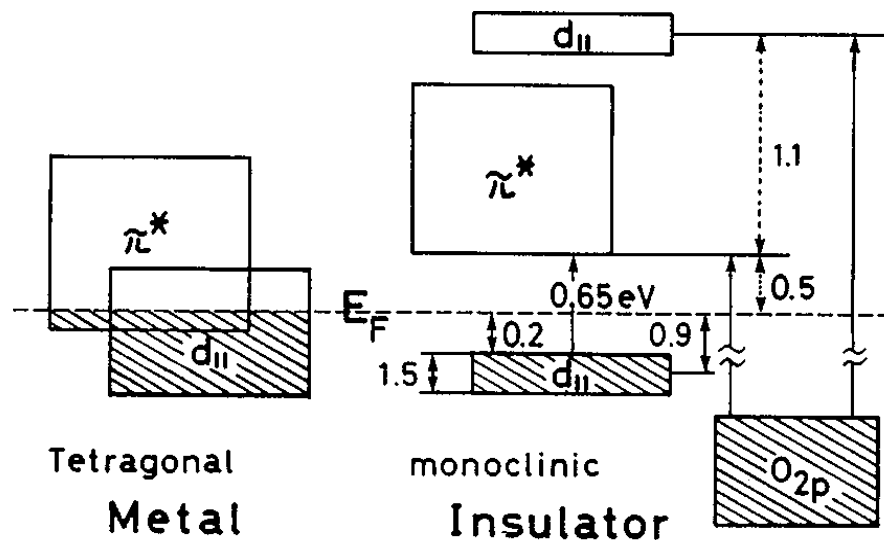

Figure 1.3. The electronic band structure of metallic and insulator VO_2
(Source: Imada, Fujimori, and Tokura 1998)

1.2.3. Phase Diagram in VO_2 Structure

Various stress/strain along the c_R axis or doping trigger to take place different phase of VO_2 material (Marezio et al. 1972, Gu et al. 2010). Figure 1.4 shows strain-temperature phase diagram of VO_2 structure. Due to compressive strain/stress, the phase transition of VO_2 actualizes from the M_1 phase to the R phase. This transition abruptly occurs. Additionally, transition temperature changes under the effect of strain and compressive strain in the c_R axis. The nucleation of guest material (R phase) inside the host material (M_1 phase) causes the inception of the transition. The new phase proceeds to consist with increasing temperature and terminate the host material. Thus, phase transition is realized. It is thought that some defects and vacancies can assist the nucleation of the guest phase. The transition of VO_2 thin film depends on an intermediate region which is called as the percolation region. In percolation region, the percolation threshold occurs, and metallic islands place in the M_1 phase of VO_2 could be connected. This case ensures a macroscopic path in terms of electrical conduction. In addition, electrical conductivity of VO_2 enhances, and a remarkable deflection takes place (Nazari et al. 2011). The sluggishness for M_1-R transition could be connected to percolation region. Moreover, tensile strains in the c_R direction the M_2 and M_3 intermediate phases of VO_2 material whereas compressed strain M_1-R transition occurs. The phase transition of VO_2 from M_1 phase to R phase broadly generates. The increasing of tensile strain leads to decrease the temperature at which intermediate phase start to enlarge. For the M_3 phase, the alignment of V-V chains take places a stress series by contrast with abrupt transition. M_1-M_3 phase transition is different from M_1-M_2 phase transition which abruptly occurs. In the event of M_1-M_3 phase transition, it is observed that there is gradually and continuously transition (Atkin et al. 2012).

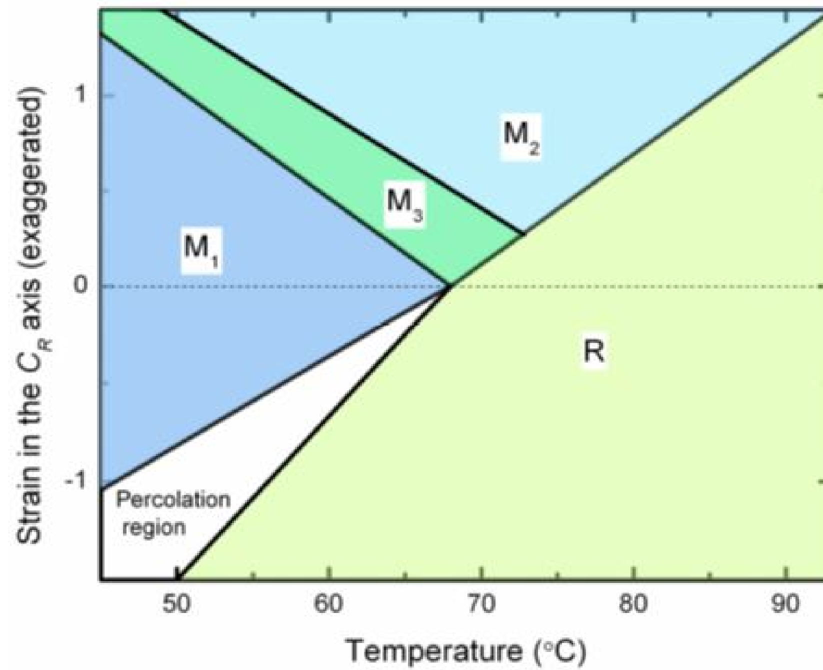

Figure 1.4. Strain-temperature phase diagram of VO_2 material (Source: Nazari 2013)

1.2.4. Phase Transition in VO_2

1.2.4.1. Mott-Hubbard Transition

In a Mott insulator, electron-electron correlation effect is an important factor in order to describe the phase of the material. According to ordinary band theory, electron configuration is not an essential factor in the description of electronic structure. There are two different electronic configurations as this view in Figure 1.5. In fact the electrons move in order to avoid inconvenient configuration as shown in Figure 1.5b. Because of disregarded electron-electron correlation, the overestimated ground state energy is known as “correlation energy” (Zallen and Penchina 1986). In the Mott insulator, it is feasible to have localized electronic wave functions owing to electron-electron correlation effects. In very broad band which has the value of Coulomb repulsion U (correlation energy) is lower than 3d bandwidth W, the reaction is realized, and it is observed conductibility. This reaction has two electrons in a system with one electron per atom. Otherwise, the level of the repulsion energy which has the value of Coulomb energy U is higher than W value is enough to split 3d band as lower filled and higher empty bands. This situation generates insulator structure.

For correlated electronic system, band structure is calculated by Hubbard Hamiltonian. In this view, two different characteristic energies are presented: first one is that the tunneling term is shown as "*t*". This term depends on the kinetic energy of the electrons, and define the tunneling of the electrons to the nearest atomic site. The other one is Coulomb (correlation) energy *U* defines the interaction energy of the electrons. In case of high value of *U/t*, Hubbard band splits into lower and upper, and this situation presents localized electronic wave functions. Thus, the system becomes insulator. The electrons with t term depends on correlation effect could not be under repulsive force effect, and the electrons occupy on site. After that, the electrons move from an atomic site to the nearest neighbor atomic site, and this cause delocalized electronic wave functions. Figure 1.6 indicates one dimensional atomic site with lower and upper Hubbard bands.

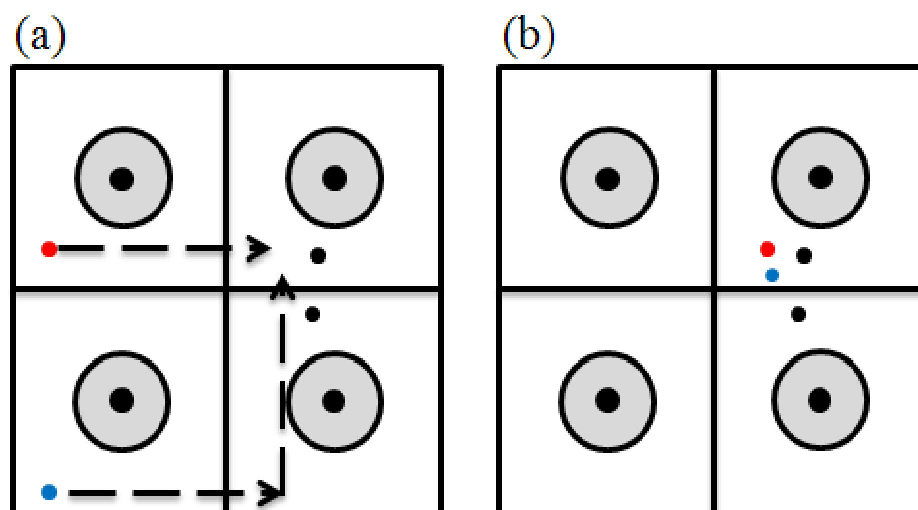

Figure 1.5. Two different electronic configurations in 2-Dimensional crystal it has (a) lower (b) higher energy because of Coulomb repulsion (Source: Nazari 2013)

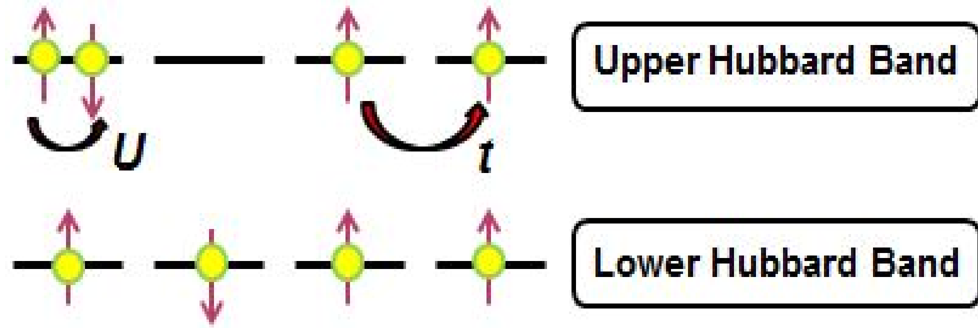

Figure 1.6. The schema of 1-Dimensional chain with one electron per unit cell with lower and upper band

For a strongly correlated system, MIT a critical on-site Coulomb energy U_C, U/U_C = 1. U refers to the on-site Coulomb energy between the electrons. Actually it is not clear whether this transition suddenly or continuously takes place (Zhang, Rozenberg, and Kotliar 1993). By Morin, it is observed that this transition depends on temperature is first-order MIT (Morin 1959). Abruptly realized MIT corresponds to a Mott transition (first order) (Morin 1959) whereas continuously realized MIT corresponds to Hubbard MIT (second order) (Kim et al. 2004). Band gap between sub-bands in the main band is broken down in the event of MIT. The band gap occurs due to U term energy. According to Mott, when the value of a lattice constant is larger compared to the critical value, MIT abruptly realizes (Mott 1990). By Brinkman and Rice (BR), it is shown as theoretical an abrupt MIT near U/U_C = 1 as strongly correlated metal with the electronic structure of an electron (Brinkman and Rice 1970). This situation is known as Brinkman-Rice (BR) picture. In addition, the extension of BR picture developed MIT via band filling (Kim 2002). This situation is known as extended BR picture. According to the measurements in an inhomogeneous metallic system, extended BR picture was based on a fractional charge (Kim 2002). At the same time, according to Hubbard, in the event of the overlapping of the sub-bands below U_C, density of states which is a finite minimum at Fermi energy level increases depends on decreasing U, and this system becomes metallic. This process belongs to continuous MIT which is presented by Hubbard. After that, continuous MIT was approved for an infinite-dimensional Hubbard model (Zhang, Rozenberg, and Kotliar 1993).

As a new method in order to observe Mott transition, a spectral weight value in k-space is determined in an inhomogeneous correlated metallic system with two region which include metallic phase and insulator phase. Nevertheless, inhomogeneous phases

are not understood from determined spectral weight. A reverse transformation from k-space into real space is not detected as shown in Figure 1.7a. This figure shows that k-space and real space are not equal to each other as mathematically. Inhomogeneous system is not similar with metal which includes an electronic structure of one electron per atom and mathematical equivalence between k-space and real space. In order to solve this problem taken data to be averaged data is considered (Kim et al. 2004). In the event of measured inhomogeneous system, carrier particles should be strike an average over lattice in the whole region. After that, the system converts to homogeneous from inhomogeneous with the electronic structure of an effective charge per atom as shown in Figure 1.7b. Effective charge is observed as $\grave{e} = \rho e$, where $0 < \rho = n/L \leq 1$ corresponds to band filling, n is known as the number of carrier density, and L refers to the number of total lattice for measurement region. In the case of just measured inhomogeneous system, the fractional effective charge is proved right. The fractional coulomb energy is described as $U \equiv < \grave{e}\grave{e} / r > = \rho^2 U_{true}$, where U denotes effective Coulomb energy and U_{true} denotes true Coulomb energy. For a putted forth U_C, U_{true} is equal to κU_C value. Correlation strength which is used in the BR picture is shown as κ (Brinkman and Rice 1970). Therefore, U is described as $U = \kappa\rho^2 U_C$. In an averaged system including an effective charge per atom, m^* denotes the effective mass a quasi-particle, and it is calculated with Gutzwiller variational theory as shown in equation (1.1) (Kim 2002)

$$\frac{m}{m^*} \equiv \frac{1}{1-(\frac{U}{U_c})^2} = \frac{1}{1-\kappa^2\rho^2} \quad (1.1)$$

In equation (1.1), m refers to bare electron mass. In addition, U/U_c is $\kappa\rho^2 \neq 1$, and in the event of $\rho = 1$ and $0 < \rho \leq 1$ which is correspond to band filling state, κ refers to the strength of Coulomb energy between carrier charges as shown in Figure 1.8. In an inhomogeneous system, equation (1.1) indicates the effect of calculation and the average of the trues effective mass in the BR picture if $\rho \neq$ (Kim 2002). At the same time; electric conductivity is described as σ is proportional to $(m^*/m)^2$. This equalization describes the extended BR picture. For equation (1.1), the material in the event of $\kappa\rho^2 = 1$ can be supposed as a paramagnetic insulator that is Mott insulator. The metal which has critical ρ value below unity indicates the best metallic properties (Tokura et al.

1993). The transition from metallic phase which has $\kappa\rho'^2 \neq 1$ to insulator phase which has $\kappa\rho^2 = 1$ abruptly realizes. This case lead to observe the Mott transition near $U/U_c = 1$. Holes are related to the variation between ρ' and $\rho=1$, and electric field with free holes induces these holes in valence band. The existences of free holes demonstrate the vanishing of the electrons, and this leads to decrease Coulomb energy. After that, the energy gap is disrupted, and inhomogeneous metallic system occurs because of the induced holes. There may be nearly 3.0 x 10^{18} cm^{-3} critical induced hole n_c (Stefanovich, Pergament, and Stefanovich 2000), as forecasted by Mott from the Mott criterion $n_c^{1/3}\alpha_0$ is around 0.25 (Mott and Transitions 1990). α_0 denotes Bohr radius. Additionally, induced hole correspond to nearly 0.018% of the number of carriers in the half-filled band in case of one electron in the cell volume. This idea is demonstrated in Figure 1.8.

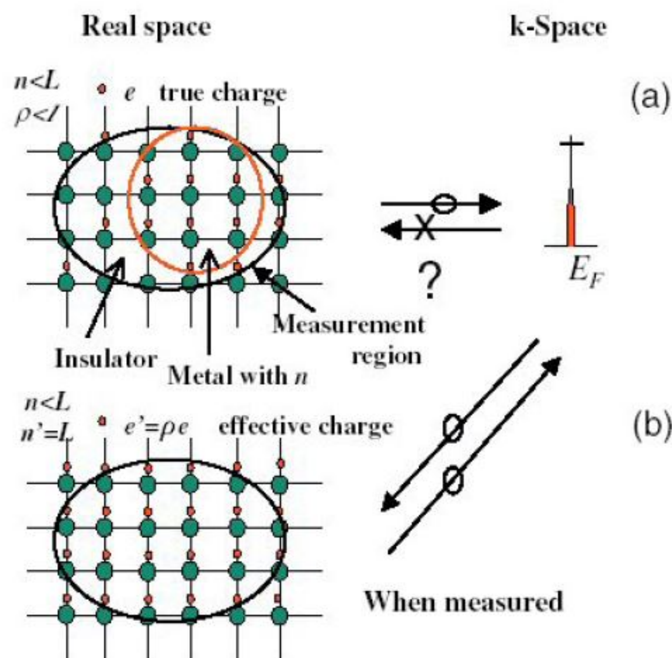

Figure 1.7. (a) A reverse transformation from k-space to real-space for an inhomogeneous system (b) when averaged over lattice, the state of being of homogeneous system from inhomogeneous system (Source: Kim et al. 2004)

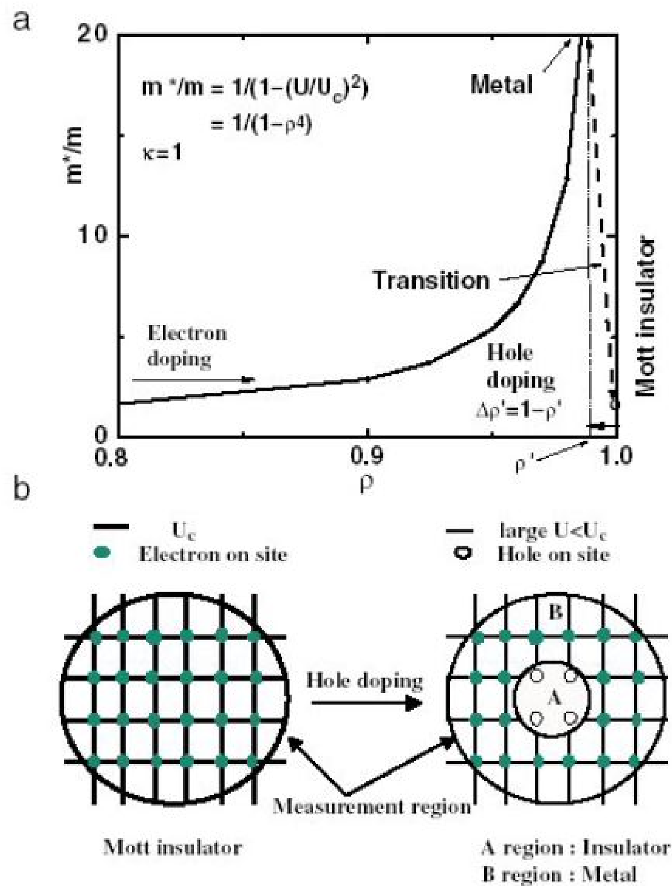

Figure 1.8. (a) The curve of the effective mass of quasi-particle (b) Mott insulator-metal with hole doping (Source: Kim et al. 2004)

1.2.4.2. Peierls Transition

In Peierls mechanism, the crystal structure can be deformed by electron-phonon interaction, and this lead to be presented a new periodicity. The ordinary band theory presents a half-full valence band for a one-dimensional chain with one electron per the atom. The lattice distortion can be generated due to electron-phonon interaction, so this interaction causes the doubling of the lattice constant. Figure 1.9 (Nazari 2013) shows schematic description of Peierls MIT. When there is no electron-phonon interaction, the chain corresponds to metallic phase which have homogenous electronic charge distribution. The atoms can be dimerized with electron-phonon interaction. In the Peierls transition, electron-phonon interaction takes place at specific temperature (T_{MIT}). The interaction leads to soften the phonon in the Brillouin zone of metallic phase. Phonon mode is affected by the interaction. Additionally, phonon softening causes the

increasing of the vibrational entropy, and plays an important role as the driving force for MIT (Gebhard 1997).

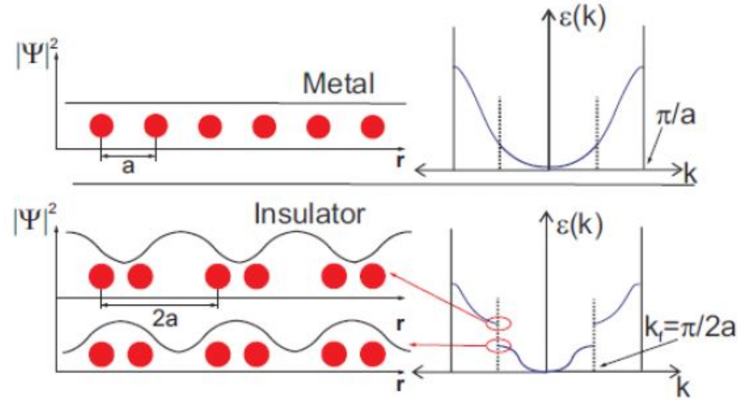

Figure 1.9. Schematic description of Peierls metal-insulator transition in a linear chain (Source: Nazari 2013)

1.3. The Applications of VO_2

1.3.1. Multifunctional Artificial Muscles

Vanadium dioxide has high Young's modulus that is about 140 GPa and transformation strain with 1-2% in single crystal. For VO_2, metal-insulator transition takes place time interval of a few picoseconds. In addition, for VO_2 single-crystal because of this transition, the volumetric density of this material is ~7 J/cm^3 that is larger by a factor of a thousand compared to human muscle. The reason of these properties, VO_2 is an ideal material for multifunctional artificial muscles (Liu et al. 2014).

1.3.2. Thermochromic Smart Windows

The smart windows are the systems which perceive and respond to light, heat or electricity. These windows can control sun light transmission. At low temperature (<70 ºC) VO_2 due to insulator phase transparent to infrared radiation, and at high temperature (>70 ºC) it becomes opaque to infrared light due to metallic phase. Because of this phase transition property, VO_2 is an attractive material for smart windows. Thus,

thermochromic windows allow the control transmission of sun lights depending on the ambient temperature (Jiang et al. 2014).

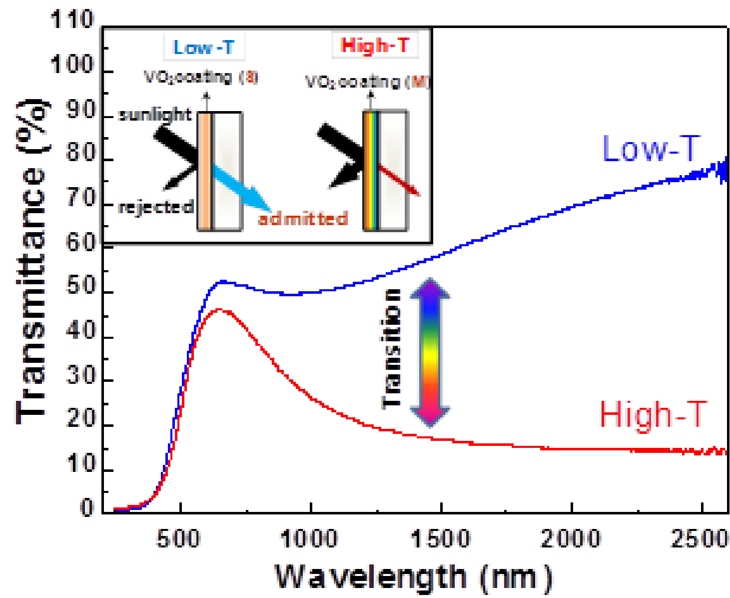

Figure 1.10. VO_2-based smart windows
(Source: Du et al. 2011)

1.3.3. Infrared Detectors

Temperature coefficient of resistance (TCR) is very important factor for infrared detector performance.

For thermal sensitive material, TCR is evaluated as (Figure 1.11):

$$\alpha = \frac{\Delta R}{R \Delta T} \tag{1.2}$$

The resistance of material changes as a function of temperature. In order to determine detector performance, not only TCR value also detectivity (D^*), responsivity (R_v) and thermal time constant (τ) are significant parameters. In the equation (1.3), G and C denote respectively thermal conductance and thermal capacity. In addition, where η is infrared absorptivity; $I_b$is bias current applied to device; R_0 is bolometer resistance at room temperature; A_d is effective absorption area, Δf and V_n

stand for respectively bandwidth and signal noise in the equations (1.4, 1.5) (Wang et al. 2013, Chen et al. 2001)

$$\tau = \frac{C}{G} \tag{1.3}$$

$$R_v = \frac{\alpha\eta I_b R_0}{G\sqrt{1+\omega^2\tau^2}} \tag{1.4}$$

$$D^* = \frac{R_v\sqrt{A_d\Delta f}}{V_n} \tag{1.5}$$

Vanadium oxide has high TCR value larger by a factor 5-10 than most metals, and it has lower noise than some semiconductors such as YBaCuO (Chen et al. 2001). Vanadium dioxide (VO_2) doped with a small amount of vanadium pentoxide (V_2O_5) exhibits high TCR value. VO_2 shows sharp transition at 70 °C. When it is doped with some other species such as V_2O_5, Au and V_2O_3 (Smith et al. 2014, Wang et al. 2013, Kumar et al. 2003) While VO_2 exhibits a fast metal-insulator transition at nearly 70 °C, the other material slows down this sudden transition. Then, the resistance of this component shows large changing with a few changes in temperature. Because of this reason, the detector senses every different temperature. Considering this properties, vanadium oxide films exhibit high performance for the bolometer.

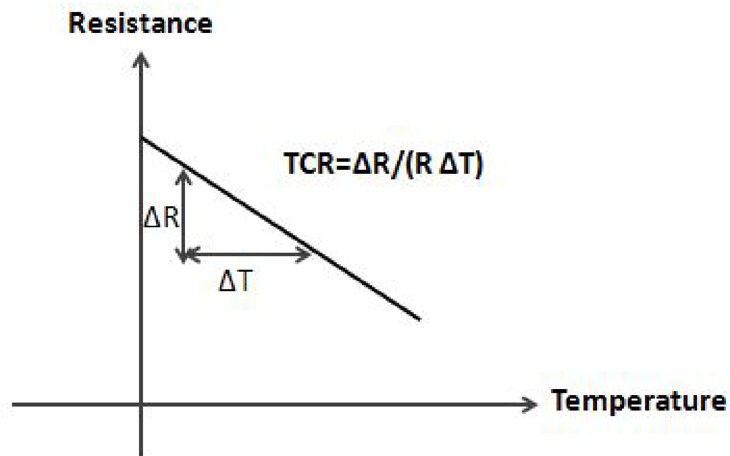

Figure 1.11. TCR measurement scheme

1.3.4. Field Effect Transistors (FET)

At room temperature, high voltage induces MIT in VO_2. Actually, it is not clear whether high voltage or local heating causes phase transition (Ruzmetov et al. 2010). To decide the reason of this transition is whether electric field or local heating is the basic reason of the transition, and it will allow differentiating between contesting theories of the MIT in VO_2. Due to current heating, generated difficulties when a 2-terminal device is under electric field can be removed with working on 3-terminal devices, such as FET. The substantiation of 3-terminal FET with VO_2 which is channel material demonstrated to be a challenging task (Figure 1.12) (Ruzmetov et al. 2010). VO_2 is a channel material between source (S) and drain (D) in FET device, and utilizing MIT property of VO_2 material, the current from source to drain can be controlled.

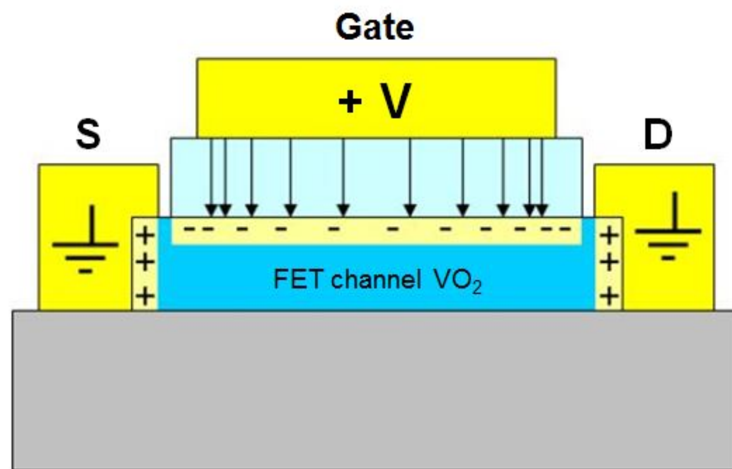

Figure 1.12. A diagram of field effect transistor (FET) device

1.4. Contents of This Dissertation

This dissertation in the next chapters will present an overview of process in VO_2 growth and the physics behind the phase transition. Thin film growth processing and VO_2 growth technique will be presented in Chapter 2. Chapter 3 is a systematic study of VO_2 fabrication and characterization technique. Moreover, this chapter provides experimental procedure with its experimental techniques. Chapter 4 will be a discussion of the effect of oxygen concentration and thickness on fabricated VO_2 thin film. Also, the chapter includes the discussion, which is about metal-insulator transition in VO_2

strips after electron beam lithography process. Finally, Chapter 5 summarizes the results as the conclusion in this dissertation.

CHAPTER 2

THIN FILM GROWTH PROCESSING

2.1. Thin Film Growth

Thin film refers to the layer of a material on a substrate, and the thickness of the substrate changes from nanometer order to a few of micrometers. Because of the applications of thin film such as optical-electrical device or wear resistance, thin film technology was used in a wide variety of areas which are microelectronics, medical and military industries.

Thin film deposition process requires three basic steps. One is fabrication of suitable atomic, molecular or ionic species required for deposition. The other one is the transfer of these species to the substrate. The last one is cohesion these species on the substrate by directly chemical and electrochemical reaction.

Production of thin film takes place with nucleation and growth processes. According to experimental and theoretical results, thin film deposition process occurs in steps as follows:

1. The ions originated from the source heat the substrate surface and lose their kinetic energies. Thus, they collected on the surface on the substrate.
2. The collected particles on the substrate surface are not in thermal equilibrium. Thus they move on the surface and form nuclei.
3. As time goes on the number of the particles attached to the nuclei increases and the nuclei starts to grow. After the nuclei reach the critical size, they become thermodynamically stable and this stage is called as nucleation stage.
4. There are several nuclei grown on the surface of the substrate and they form islands.
5. Formed islands continue to grow, and they start to coalesce. In this step the combination of the small islands creates the bigger islands and this stage is called coalescence stage.

6. Larger islands continue to grow, and because of this reason, they form a thin film on the substrate surface. However, at the boundaries of the islands there occur discontinuous in the thin film.

Thin film growth techniques include physical and chemical processes such as glow discharge, reactive sputtering techniques. By sputtering deposition technique, thin film with thickness from few nanometers to several micrometers can be fabricated (Wasa, Kitabatake, and Adachi 2004). There are common used four type sputtering methods which are DC, RF, reactive and magnetron sputtering.

2.2. Sputtering Method

The atoms from the surface of a target are ejected with gas particles by bombardment. This case is called "sputtering". Sputter deposition is a physical vapor deposition (PVD) method among thin film deposition methods. Also, sputtering is one of the most used methods in order to fabricate thin films. In addition, it is a momentum exchange which is between the ions and atoms in the materials because of collisions. The ions which have high energies in the plasma directed by a strong electric field to the surface of the target. Thus, the collision between the plasma ions and the surface of the target causes to eject of the atoms, and these ejected atoms are deposited on the substrate surface as shown in Figure 2.1.

The advantages of magnetron sputtering technique were presented as follows:

1. Ejected atoms strongly adhere on the film substrate.
2. Deposited films have good thickness uniformity.
3. Growth processes can be controlled easily.
4. It is deposited to large areas with good quality and uniformity.

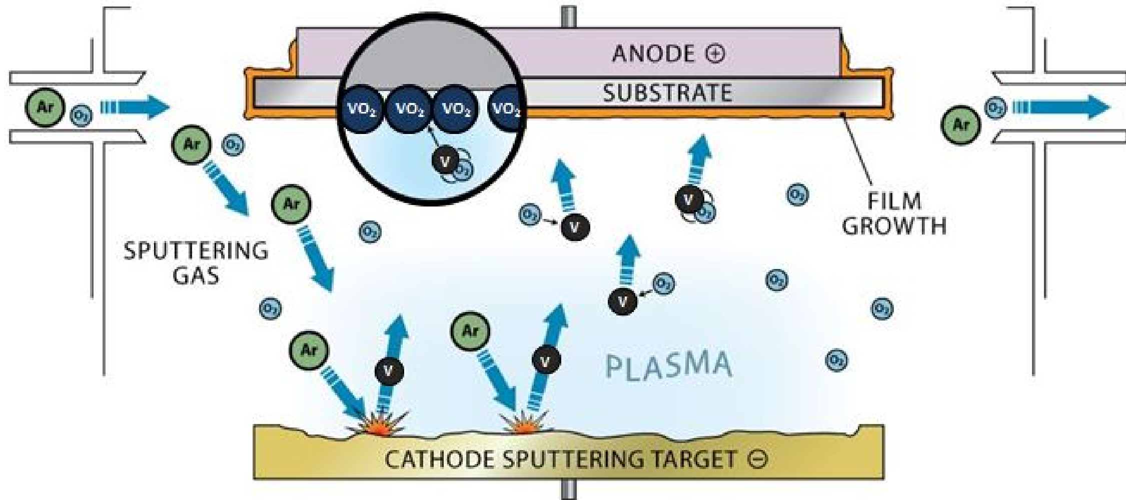

Figure 2.1. Sputtering schema

2.3. Plasma

As chemically, reactive plasma discharge is used in order to functionalize the surface of a material and improve their properties. The largest producing industries in the world acquire some advantages owing to using plasma processing technology. Surface mechanism which bases on plasma technology is applicable for the purpose of manufacturing integrated circuits which is used in electronics industry (IC) and the other processes such as textile, aerospace, automotive, food, and a pot of for biomedical industries.

5The fourth state of matter is called as plasma, and plasma is electrically neutral. Plasma consists of free electrons and moving charged particles. Because atoms or molecules release their valence orbit electrons, and these electrons become positive charge electrons. In the event of increasing temperature or increasing the energy level of gas atoms, a number of atoms become ionized so that they can participate in plasma situation. Plasma state stands in equilibrium due to the fact that the number of negative and positive charged particles is almost equivalent. The parameters which define plasma are temperature, the density of electrons and the density of particles or neutral atoms. In addition, the temperature of the electrons in plasma state is usually higher than the temperature of the ions. Lastly, glow discharges have some properties as follows:

1. Glow discharge is sustained by electric field.

2. Glow discharge is created due to the fact that charged particles collide with neutral gas atoms.
3. At the surface, glow discharge becomes neutralized.
4. The ionization of neutral gas molecules maintains plasma process.
5. There is no thermally equilibrium between the electrons and the ions.

In order to create plasma, ionization is necessary. Plasma density generally relates to electron density which is the number of free electron per unit volume. A small amount of ionized gas can generate plasma. The degree of ionization is described as;

$$\alpha = \frac{n_i}{n_n + n_i} \tag{2.1}$$

Where α is the degree of ionization. n_i and $n_n$stand for respectively the density of charged particles in plasma state and the density of neutral gas in the equation (2.1).

2.4. Atomic Collisions

There are some events which have happened in case of two particle collisions. Because of this collision, neutral particles may be ionized, and ionized particles could be neutral. This situation causes the change in the momentum of the particles (Lieberman and Lichtenberg 1994). This collision becomes as elastic or inelastic. For the elastic collision, the total kinetic energies of these particles after and before collision process are conserved. That is, the total kinetic energy is redistributed between only these particles, and the directions of these particles change. For the inelastic collision, the internal energies of these particles which collides the other particle change, and the particles have different energy level as before the collision. Thus, the total energies of these particles after and before collision process are not conserved. In addition, this situation causes the change in the vibrational or rotational states of these particles.

Transportation phenomena in gases or ionized plasmas can be explained by elastic collisions. Colliding particles block free motion of the particles. In this case, these particles are scattered by the other particles. This scattering highly affects the motion of the particle. Therefore, the transportation of particles, momentum or energy

can be explained by effective cross section for the scattering of the particles at large angles. Additionally, the mobility of the ions depends on the effective cross section for the ion scattering. The mobility of electrons in a gas atoms or the electrical conductivity of ionized plasma can changes under the effect of cross section for scattering electron. In the event of the scattering of atoms or molecules with their thermal energies, the elastic cross section refers to gas-kinetic cross section. The value of this sections is around 10^{-15} cm^2, and gas-kinetic cross section identify the mean free path for a particle.

2.5. Nucleation and Growth

Due to exposing atomic flux originated a sputtering target, thin film is grown on the surface of a suitable substrate. In a vacuum ambience, molecules and atoms with their momentums are absorbed on the surface of the substrate. Any particles which come close to the substrate surface are interacted with surface atoms. When the atoms lose their energies because of this interaction, the energy of the sputtering atoms cannot be sufficient in order to escape from the surface, and these sputtering atoms are trapped on the surface. This case is termed as the process of physisorption. Physisorption which is physical adsorption includes weak bonds like Van der Waals. The energies of these type bonds are around 0.01 eV. When the molecule acquires sufficient energy, it can diffuse across the surface and desorb. If not, this molecule could interact with the other surface atoms and create chemical bonds. This process refers to chemisorption. Chemisorption which is chemical adsorption includes chemical bonds like strong bands. The energies of these type bonds are about 1.0-10 eV. Adsorption is a surface base process in which adsorbate film is formed on the surface.

The surface diffusion steps are significant in order to provide an adsorbed atom sites to settle at the lowest energy level. There are three types of thin film growth modes as shown in Figure 2.2 (Taşdemir 2015), thin film atoms are strongly bound to each other while they are weakly bound to the substrate. It is observed slow diffusion. Lastly, for Stranski-Krastanov growth, the mixture type of these two types is also possible. This cause to create mixed type that is known as Stranski-Krastanov growth. There is the change in energetics.

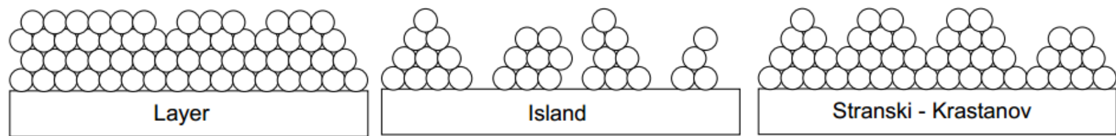

Figure 2.2. The image of the various thin film growth modes
(Source: Taşdemir 2015)

2.6. Deposition on Sample

Vacuum ambiance is provided in an appropriate reservoir like vacuum chamber which include all tools above. A gas without charge gets in vacuum ambiance to create plasma. In order to prevent chemical reaction in vacuum system, inert gas is preferred. Nevertheless, to obtain different phases which are difference from target material in some applications, chemical reaction is requested, and a reactive gas is used to occur plasma. For sputtering process, Argon (Ar) is mostly used. The first ionization potential of argon is 15.7 eV, and the second ionization potential of argon is 27.76 eV. According to calculations, the mean free path of argon is nearly 8 cm at 1 mTorr at room temperature. Nitrogen (N_2) or oxygen gas atoms may cause reactive sputtering in the event of the entries of these reactive gas atoms with argon atoms in vacuum ambiance. Because of the fact that there is a potential difference between anode and cathode slabs, electric field carries out this area which is between anode (sputtering source) and a cathode. Negative voltage causes electric field from anode to cathode. At room temperature, the gas atoms include a small amount of the ions and several free electrons. When the gas atoms start to enter in vacuum system, electric field lead to the acceleration the ions and electrons respectively the anode and the cathode. Then, in addition to more electrons and ions which carry out due to the collisions of the electrons with gas atoms, new electrons form on the cathode surface. The electrons actualize tunneling process from the cathode to the ions, at the ions become neutral. In case of neutralized ions, the ions release their energies. Then, this ionization energy may be given to surface electrons with Auger process. In the event of high energy transfer, the atoms ionize, and accelerate toward the cathode. These electrons are called as "secondary electrons". Under electric field effect, these electrons accelerate, and this

leads to new ions and free electrons take place. When applying sufficient power, plasma is created. The plasma regulates itself temperature, density and distribution up to achieving a balance between the lost charge and applied energy. There may be collision between the electrons and neutral species. When energy transfer is insufficient compared to the ionization potential energy, the atom can be excited to the higher energy levels. The atom passes on from excited state through optical transition, which provide glow (Venables 2000).

2.7. The Mean Free Path

In the event of collisions in vacuum system, a particle moves in specific region. In the region, average traveled distance is called as the main free path. It decreases as depending the increasing of vacuum pressure due to the fact that the density of gas molecules increases. In accordance with kinetic theory, there is no any interaction between gas atoms in the case of the collisions. The atomic sizes of gas atoms are different from each other. The atomic sizes of gas atoms are high, which causes to increase the probability of collisions, and decreases the mean free paths of the atoms. Also, the proportions of energy transfers depend on atomic collisions and the mean free paths of the atoms. As considering this information, the particle move along a straight line in a unit distance of the mean free path of the atom.

2.8. Sputter Yield

The sputter yield (S) which is the ratio of the numbers of directed ions to the removed atoms from the target surface as given equation 2.2.

$$S = \frac{removed\ atoms}{incident\ ions} \qquad (2.2.)$$

Factors affecting the sputter yield are energy of the incident ions, the properties and the crystal structure of the target material. There are several methods in order to

measure sputter yield (Wasa, Kitabatake, and Adachi 2004). The methods are presented as follows:

1. Measure the decreasing in the thickness or weight of the target.
2. Determine how much material deposited on the substrate.
3. Detect scattered particles in the system.

2.9. Sputtering Systems

2.9.1. Direct Current (DC) Sputtering

For DC sputtering system, the plasma is generated by using DC power source. The plasma is produced between a cathode and an anode plates with sufficient gas pressure and electric field which is enough to ionize the gas. The positive gas ions accelerate and hit the cathode plate, so the hitting produces secondary electrons. In addition, these secondary electrons scatter back and collide with gas particles and ionize them also. This plasma consists of free electrons and positive gas ions and these positive gas ions are used bombarding the target. The disadvantages of DC sputtering are low deposition rate, and this sputtering is not suitable for insulators.

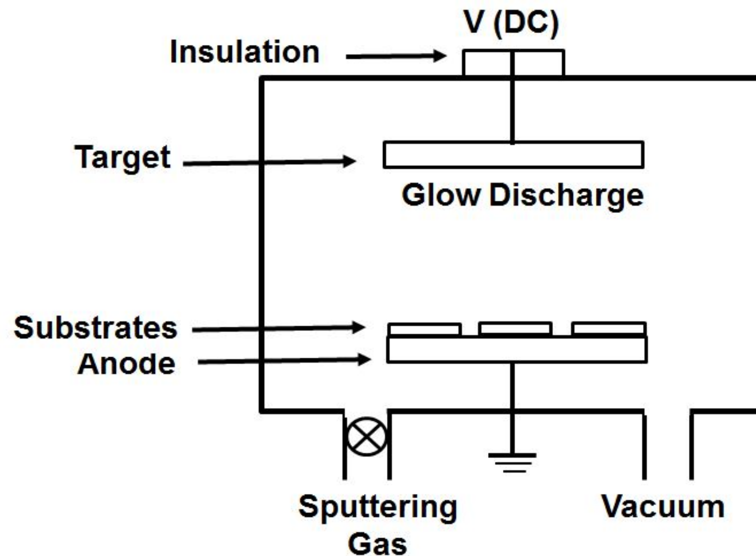

Figure 2.3. The basic system of the DC sputtering

2.9.2. Radio Frequency (RF) Sputtering

The working principles of the RF sputtering are similar to the principle of DC sputtering. However, in the RF sputtering a radio frequency power source is used instead of a DC source. In the event of the fact that the plasma ions hit the target, the electrical charge of the plasma ions become neutral, and these neutralized ions turn back the process as atom. However, when insulator target is used for sputtering, neutralization process carries out with positive charge on the surface of the target. This charge may be cause to stop sputtering process due to bombarding ions. In order to maintain this process, the polarity must be turned back to retract sufficient electrons from the plasma for the elimination of surface charge. This periodic reversal in the polarity carries out as automatic owing to applied radio-frequency (RF) voltage on the target. The advantage of the RF sputtering is that its anode and cathode periodically change so the insulator substrates are not charged. Therefore this sputtering technique can be used for both conductors and insulators. Also, it has a higher deposition rate compared to the DC sputtering technique. Thus, this type sputtering technique is called as RF sputtering.

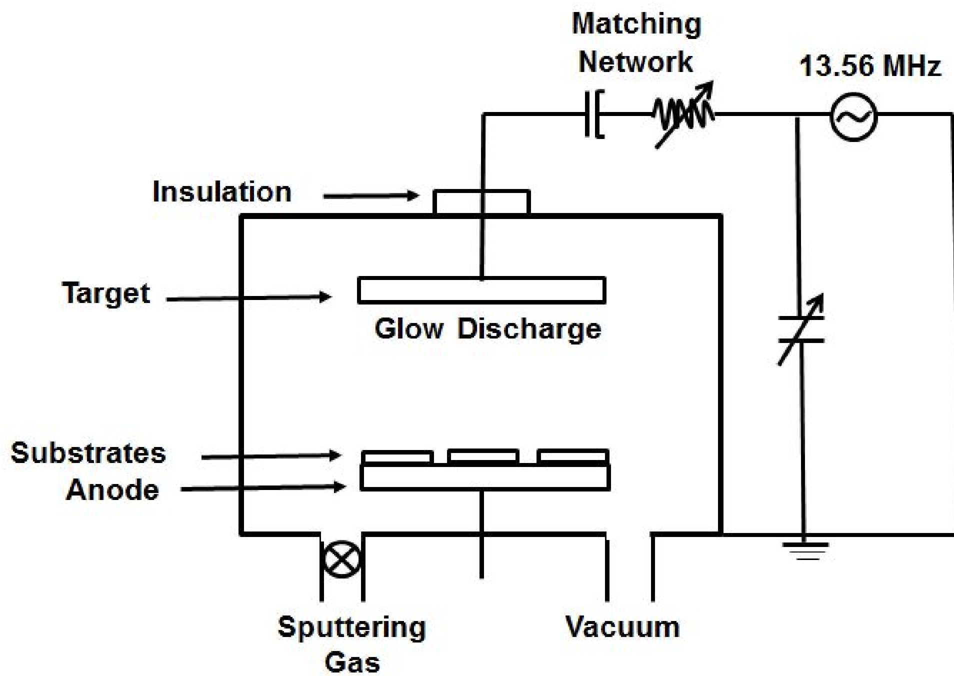

Figure 2.4. Basic elements of RF sputtering

2.9.3. Reactive Sputtering

In vacuum system, there can be chemical reactions between sputtered atoms and sputtering gas. In order to prevent these type chemical reactions, inert gas such as argon (Ar) is used for ionizations. Nevertheless, in order to obtain a chemical compound, a reactive gas such as oxygen is added to inert gas for some applications. The reactive gas reacts with the target and forms a thin film on the surface. This technique is used especially to create oxide thin films. This type sputtering technique is called as reactive sputtering.

2.9.4. Magnetron Sputtering

In magnetron sputtering technique, magnets are used in order to increase the efficiency of the magnetron sputtering process. The magnets play an important role for sputtering technique; they lead to increase the number of electrons which participates ionization processing, and increase deposition rate. The magnets which have strong force are stated behind the target in order to create magnetic field which come up to

electric field with right angle. The magnetic field and the electric field interact and lead to form electron drift path target surface, and the ions and electrons move under the influence of the Lorentz force due to specially aligned electric and magnetic fields and this process increases the probability of colliding the charged particles (improves the ionization). Therefore, deposition rate is 10-100 times faster for magnetron sputtering compared to sputtering process without magnetron configuration. Owing to magnetrons, in order to obtain ionization efficiency, less number of argon atoms is sufficient. Magnets cause the creation of more collisions and a number of the ions which lead to glow discharge simple to form. The simple creation of plasma requires lower power or voltage to be continued. This technique can be used with both DC and RF power sources so it is suitable for conductor as well as insulator targets.

CHAPTER 3

EXPERIMENTAL PROCEDURE

3.1. Purpose

The main purpose of this work is to fabricate VO_2 thin film grown on c-cut sapphire [Al_2O_3(0001)] by DC magnetron sputtering technique as a channel between source and drain for field effect transistor (FET) applications. Grown VO_2 thin films were characterized to determine structural and optical properties using various techniques such as scanning electron microscopy (SEM), X-ray diffraction (XRD), Raman microscopy, X-ray photoelectron spectroscopy (XPS) and spectrophotometer. In addition, the resistivity of the grown thin films was analyzed to determine electrical properties at various temperatures in probe station system under vacuum. After these characterizations, the highest quality VO_2 sample was given shaped by electron beam lithography in order to produce the VO_2 channel of FET device.

3.2. Experimental Process for Vanadium Oxide Thin Films on c-cut Sapphire [Al_2O_3 (0001)]

Different fabrication methods have been studied for thin-film VO_2 growth such as pulsed laser deposition (PLD) (Kim and Kwok 1994), chemical vapor deposition (CVD) (Maruyama and Ikuta 1993, Sahana, Subbanna, and Shivashankar 2002), Sputtering (Ruzmetov et al. 2007, Ko and Ramanathan 2008), sol-gel coating (Chae, Kim, and Yun 2008), electron beam evaporation (Hood and DeNatale 1991) and ion beam deposition (West et al. 2008). Each method has certain advantages and disadvantages to grow thin film.

In this work, DC magnetron sputtering technique was used to fabricate VO_2 thin film because magnetron sputtering technique provides high quality, strong adhesion, and uniformity.

The processes for sputtered grown of VO_2 thin films on sapphire substrate are presented as follows:

1. Sapphire (c-Al_2O_3) which has a good thermal conductivity (27.21 $Wm^{-1}K^{-1}$ at 300 K) was used as a substrate.
2. The substrate was cleaned respectively in acetone, methanol and propanol with an ultrasonic vibration cleaner during 10 minutes for every step. Then the substrate was dried with pure nitrogen gas.
3. 2'' Pure Vanadium (V) (99.9%) was used as a target.
4. In order to obtain a good crystal structure, the substrate was heated up to 550 ºC. At the same time, in order to provide homogeneity on the thin films, each substrate was rotated with 15 rpm during deposition.
5. While base pressure was around 3.2 x 10^{-6} mbar, deposition pressure is at nearly 8.7 mbar in the vacuum system.
6. In order to obtain VO_2 phase, Ar+O_2 mix gas was sent in vacuum system during thin-film deposition.
7. Vanadium (V) metal target was pre-sputtered for 10 minutes before thin film growth process.
8. O_2 and Ar gas mixture which was introduced into vacuum system taken place the oxidation of V sputtered particles, and grow VO_2 thin film.
9. The thicknesses of grown thin films were 125 nm and 310 nm as depending on the deposition time.
10. The structural-optical analyzes of the thin films were carried out by various techniques which are SEM, XRD, Raman, XPS and spectrophotometer.
11. The temperature dependence of resistivity of VO_2 thin films were measured in probe station under vacuum.
12. Grown VO_2 thin film was patterned by electron beam lithography for fabricating VO_2 channel.

3.3. Vanadium Oxide Thin Film Fabrication Method

3.3.1. Magnetron Sputtering System

Magnetron Sputtering System was designed to fabricate VO_2 thin film in Thin Film Laboratory at Physics Department, IZTECH as shown in Figure 3.1. When DC power is applied between V target and the substrate, electric field is generated in this area. Because of the fact that strong potential difference is applied to inert argon (Ar) gas, it causes the ionization of Ar atoms and generates plasma. The magnets under the target create magnetic field. These magnetic fields deflect scattered Ar ions leading to multiple collisions with the target. Moreover, the ionized argon atoms are accelerated by potential differences. Thus, V target atoms are ejected and move to the substrate. In this case, due to oxygen atoms with Ar gas, chemical reaction occurs between V-O atoms..

In order to heat the substrate, a heater was designed for sputter vacuum system as shown in Figure 3.1b. The substrate was heated up to 550 ºC with 4 lamps 24 V- 250 W. The substrate temperature has been controlled with PID controller device connected J type thermocouple. In addition, the substrate was rotated by rotation mechanism connected the substrate holder as shown in Figure 3.1b.

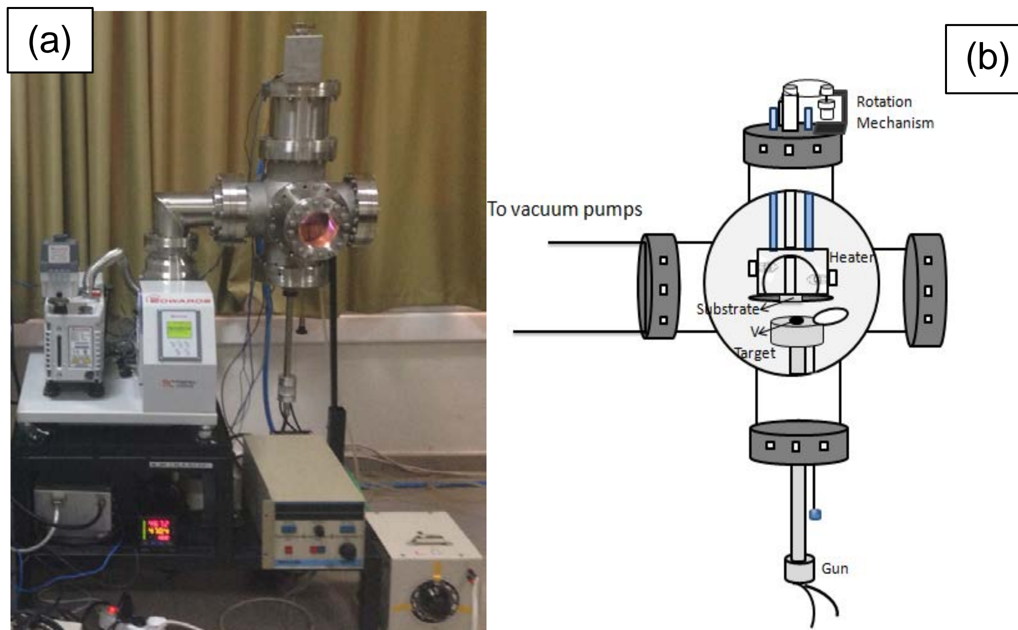

Figure 3.1. The picture of (a) magnetron sputtering system (b) growth chamber

3.4. Measurement Systems

3.4.1. Scanning Electron Microscopy (SEM)

Scanning electron microscope (SEM) generates the image of a pattern by scanning with high energy electrons which are focused on a small area.

Electron beams interact with external orbital electrons of the atoms in the sample due to Auger ionizations. These electrons include information about the surface of the sample. Due to high energy incident electron beam secondary electrons are ejected from the surface atoms. These secondary electrons reveal topographic image of the sample the energy of the electrons can vary from 200-300 eV to 100 keV. The working principle of SEM is similar to optical microscope. However, in order to obtain the image of the sample SEM uses the electron beam, optical microscope uses the beam of the light. Lastly, the electrons with high energy provide an advantage to see the sample at atomic level with higher resolution.

Structural and morphological features of grown films were examined by field emission scanning electron microscopy (FE-SEM) Philips Quanta equipped which is located at MAM of IZTECH.

3.4.2. X-ray Diffraction (XRD)

X-rays are electromagnetic radiation of wavelength around 1 Angstrom (Å), which is nearly the same the size of an atom. X-ray diffraction (XRD) is an analytical technique, and has been used to determine phase identification of a crystalline material and obtain information about unit cell dimensions. The dominant effect which is scattering of these X-rays from the atoms belongs to the target take places when an incident beam of monochromatic X-rays interact with a target. The scattered X-rays cause constructive and destructive interference in a material that has regular structure. X-ray diffraction is defined with Bragg's Law:

$$2d\,sin\theta = n\lambda \tag{3.1}$$

Where variable d is spacing between the atomic layers of a crystal; Θ is the angle of incident light; n is an integer; λ is wavelength of the incident beam in equation (3.1) (Figure 3.2) (Klug and Alexander 1954).

The phase identification was determined, and the crystallinity of the thin films was examined by XRD technique which is located at MAM of IZTECH. The XRD was operated in the Bragg-Brentano which focuses geometry from 10˚ to 80˚ on the Philips X'Pert Pro X-Ray diffractometry, and copper target was used for single-crystal diffraction with CuK_{α}=1.5418 Å using a step size 0.2˚ and a time step of 12.5 min.

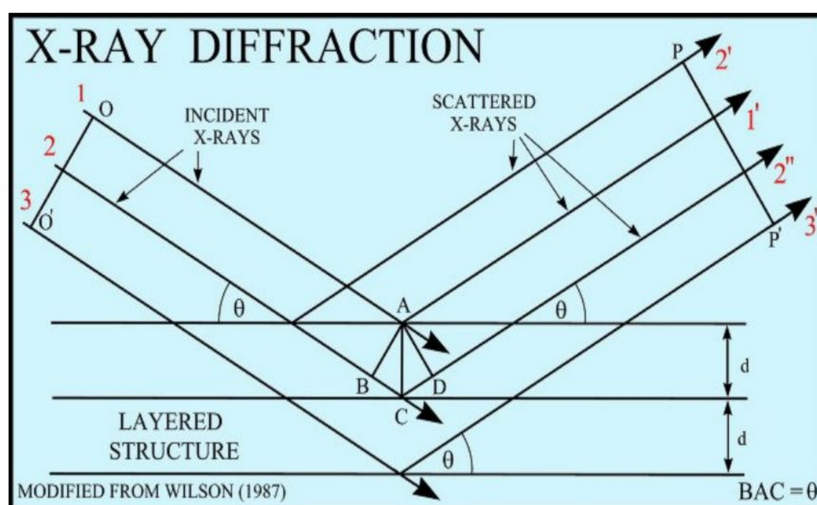

Figure 3.2. X-ray diffraction pattern (Source: Gottimukkala 2005)

3.4.3. Raman Spectroscopy

Raman spectroscopy is a spectroscopic technique that gives information about molecular vibration of the material.

When incident light is scattered from a molecule or a crystal, most of the photons are elastically scattered. The wavelength of the incident light is the same as the scattered light; this is known as Rayleigh or elastic scattering. When the wavelength of the incident light is different from the wavelength of scattered light, it leads to inelastic scattered is termed Raman effect. In Raman scattering, a small amount of scattered light is shifted in energy due to the fact that the laser light interacts with molecular vibrations or phonons (Turrell and Corset 1996).

The energy difference between the incident and scattered light is presented by numerically in equation 3.2 where $\mathcal{V}$ is Raman shift in wavelength (cm^{-1}); λ's are the wavelengths of incident and Raman scattered light.

$$\mathcal{V} = \frac{1}{\lambda_{incident}} - \frac{1}{\lambda_{scattered}} \qquad (3.2)$$

Raman analysis was carried out by confocal Raman spectroscopy with an excitation wavelength of 514.5 nm which is located in the Physics Department of IZTECH, and this technique is used to obtained vibration modes of vanadium oxide thin films.

3.4.4. X-Ray Photoelectron Spectroscopy (XPS)

X-ray photoelectron spectroscopy (XPS) is a surface sensitive spectroscopic technique which gives information about elemental composition, chemical and electronic state of containing elements within a specimen. X-ray beam irradiates the sample, and excites a bound electron to a continuum state. Kinetic energy of emitted electron is measured by the instrument and work function (Φ) depends on the spectrometer and the sample. Thus, the binding energy is obtained of the electron. This energy is a fingerprint of the atoms in the material. Each element presents a characteristic XPS peaks at binding energy values. The conservation of energy equation is presented in equation 3.3.

$$E_{binding} = E_{photon} - (E_{kinetic} + \Phi) \qquad (3.3)$$

Where $E_{binding}$ is binding energy of the electron; E_{photon} is the energy of the X-ray photons; $E_{kinetic}$ is the kinetic energy of the electron; Φ is work function of the spectrometer (Paterson and Swaffield 1994).

XPS measurements were taken with a monochromatized Mg K_{α} radiation source (hv=1254 eV) at 200 W power. The analyzer pass energy was set at 30 eV, and the step size was set at 0.1 eV. CasaXPS software was used with applying the Shirley background subtraction to do deconvolution process of spectra.

XPS data were obtained to determine chemical composition of thin films with SPECS Phoibos 150 3D-DLD located at Physics Department, IZTECH.

3.4.5. Optical Characterization

Ultraviolet/Visible/Near-Infrared spectroscopy is the quantitative measurement of the transmission, reflection or absorption of a specimen as a function of wavelength in the ultraviolet(UV)-visible-near infrared (NIR) region (Griffiths and De Haseth 2007). Spectrophotometer utilizes photometers. The intensity of a light beam as a function of its wavelength can be measured by the photometers. As using this technique, it can be obtained knowledge about spectral band gap width, the percentages of specimen transmission, logarithmic range of absorption measurement and the percentage of specimen reflectance. Light ranges vary between 200 nm -2500 nm utilizing various control and calibrations depend on the energy of the photometric determination.

PerkinElmer Lambda 950 UV/VIS/NIR spectrometer located in Dielectric Laboratory at Physics Department, IZTECH was used optical measurements.

3.4.6. Electrical Characterization

Electrical measurements were carried out in the probe station system which is located in Dielectric Laboratory at Physics Department, IZTECH as shown Figure 3.3. In probe station, resistance values of the films under vacuum were measured utilizing Keithley 2100 digital multimeter device. Additionally, the point where the sample was placed was heated up to 100 ˚C in order to observe MIT properties of the films. In addition, Labview software was designed to taken the data and control this system.

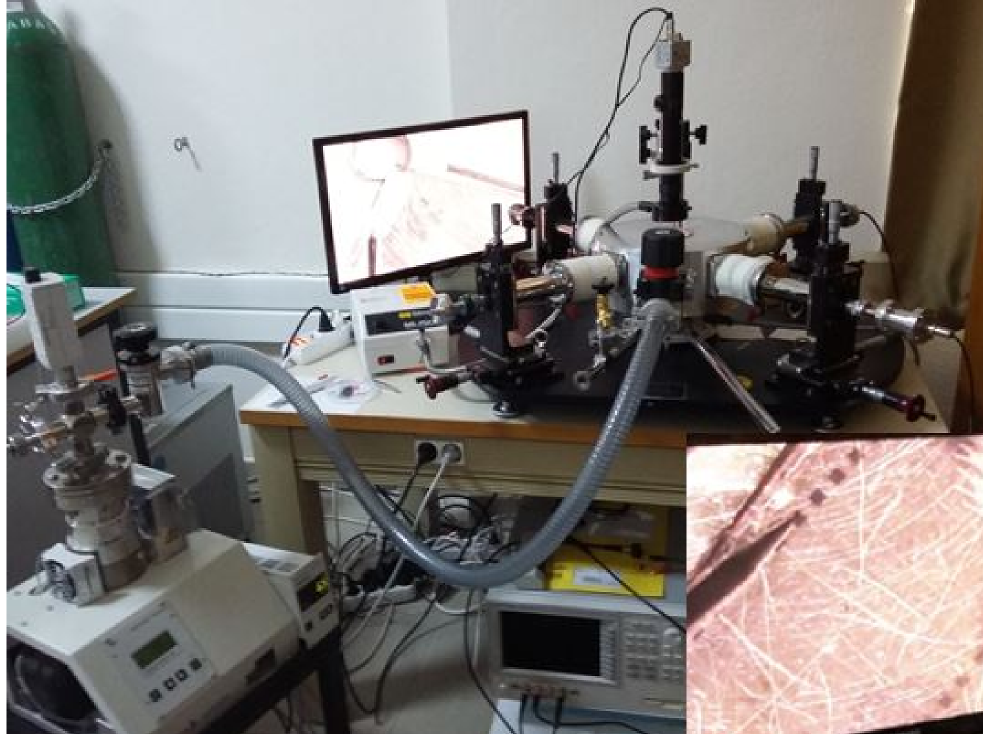

Figure 3.3. The picture of probe station

3.5. E-Beam Lithography Process of Shaped VO_2 Films

3.5.1 Clean Room Process

After VO_2 deposition process, the sample was prepared to be shaped by electron beam lithography without detriment to the crystal surface.

In clean room, deposited VO_2 thin film was coated with AZ5214 negative photoresist (PR) by spin coater. This coating takes 60 seconds, and spin coated is rotated with 3000 rpm. The thickness of this coating was around 1.5 µm resist. After this coating process, PR coated VO_2 sample was soft baked at 90 ˚C during 30 minutes in order to adhere PR on the surface. Afterwards, the sample was available to be shaped by electron beam lithography. In order to give form with electron beam, 10 kV e-beam was used. After that, the sample was exposed to UV light for 7 seconds. In order to lift off the area that the electrons was not collided, the sample was settled in distilled water and developed in NaOH (sodium hydroxide) solution during 30 seconds. Then, the sample was hard baked at 120 ˚C for 30 minutes in order to increase the durability of PR on the surface of the film. These alignments were shown in Figure 3.4.

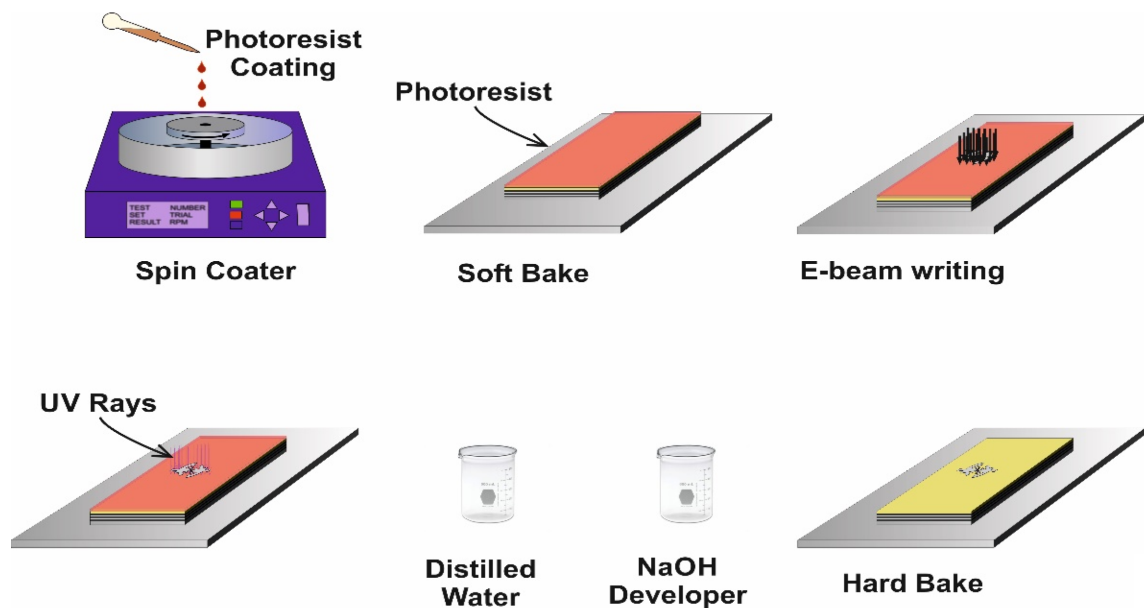

Figure 3.4. Schematic presentation of clean room and electron beam

3.5.2. Electron-Beam Lithography

Electron beam lithography (EBL) which is an important technique of nanofabrication is used to draw custom shapes on a thin film surface which is sensitive e-beam resistance. The most important advantage of this technique is drawing a specimen with sub-10 nm resolution that is below the diffraction limit of the light. Additionally, this technique provides high resolution. E-beam lithography is a method which does not require a photo mask as different from classical photolithography process. It is used to create the mask as well. However, this technique has some disadvantages such as expensive, complex system and slower exposure time compared to a photolithography system. Moreover, this process requires high vacuum condition due to charged electrons during exposure time (Demirhan 2014).

Before electron beam lithography process, the thin film was coated with negative photoresist. Then, electron beam process was carried out by e-line program as shown in Figure 3.5. UV light leads to disintegration of the photoresist molecules in the area where electron beam has not reached. After that, the photoresist was developed in NAOH developer. After that, hard bake process carried out to increase durability of PR.

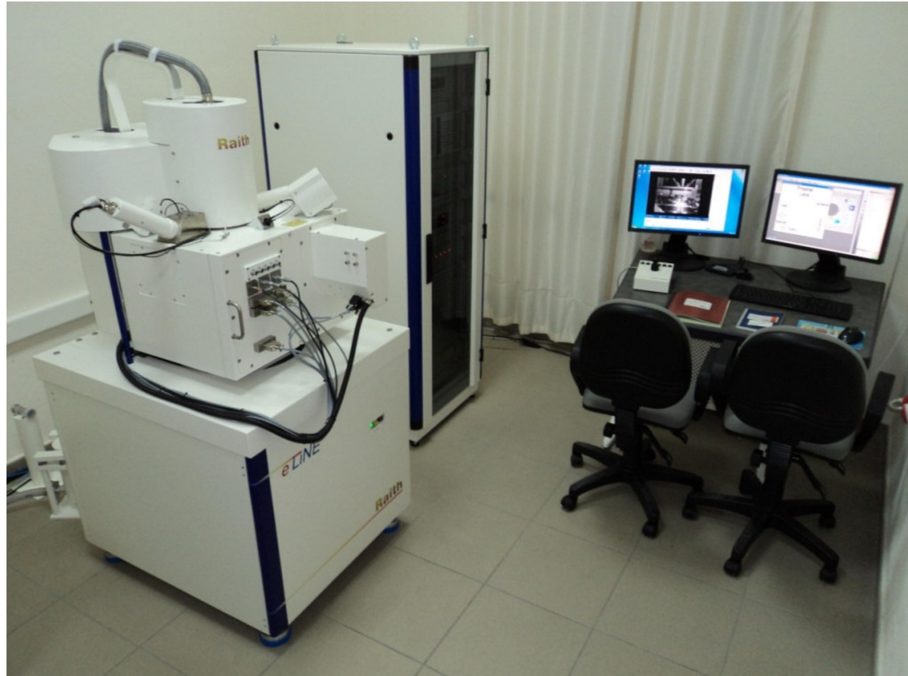

Figure 3.5. Electron beam lithography system

3.5.3. Ion Beam Etching

There are a lot of techniques to shape grown VO_2 thin films for FET production in microns such as wet, anisotropic wert and plasma etching. Isotropy and anisotropy attached to removed materials from the surface of grown thin films uniformly whole or one direction. While wet etching belongs to chemical or liquid etching, plasma etching belongs to dry gas or physical dry etching. The main difference between wet and plasma etching is etching time. The etching time of plasma etching is slower compared to wet etching.

In this system, ion source is used in order to generate broad ion beams which are directed towards the substrate during etching process. Electron bombardment leads to ionize (Ar) argon atoms in the vacuum chamber. The electrons are created and collected by cathode-anode filaments. After this, magnetic field causes the orientation of the electrons and to increase the probability of etching. In order to obtain low pressure in the vacuum system, turbo molecular pump is used with a rough pump. Ion beam plasma takes place in lower pressure, and low pressure prevent contamination of the substrate during this process.

In our study, after electron beam lithography process, the VO_2 sample was placed in argon ion beam etching system in our laboratory (Figure 3.6). Besides, this sample was placed to the sample holder with an angle of 67.5˚. Before starting etching processing, vacuum pressure slimed down up to 10^{-6} Torr as using Turbo molecular pump with the rough pump. In order to create the plasma, 30 sccm Ar gas was sent in vacuum system. Afterwards, DC voltage was applied to generate the plasma inside the etching chamber. As using rotational feed through mechanism, the sample was rotated in order to prevent the differences on the surface. Throughout etching processing, the collision between accelerated atoms and crystal atoms causes heating. Therefore, a cooling system has been used to cool the sample holder. Thus, unprotected area was etched down with this process, and we obtained shaped VO_2 channel (Figure 3.7).

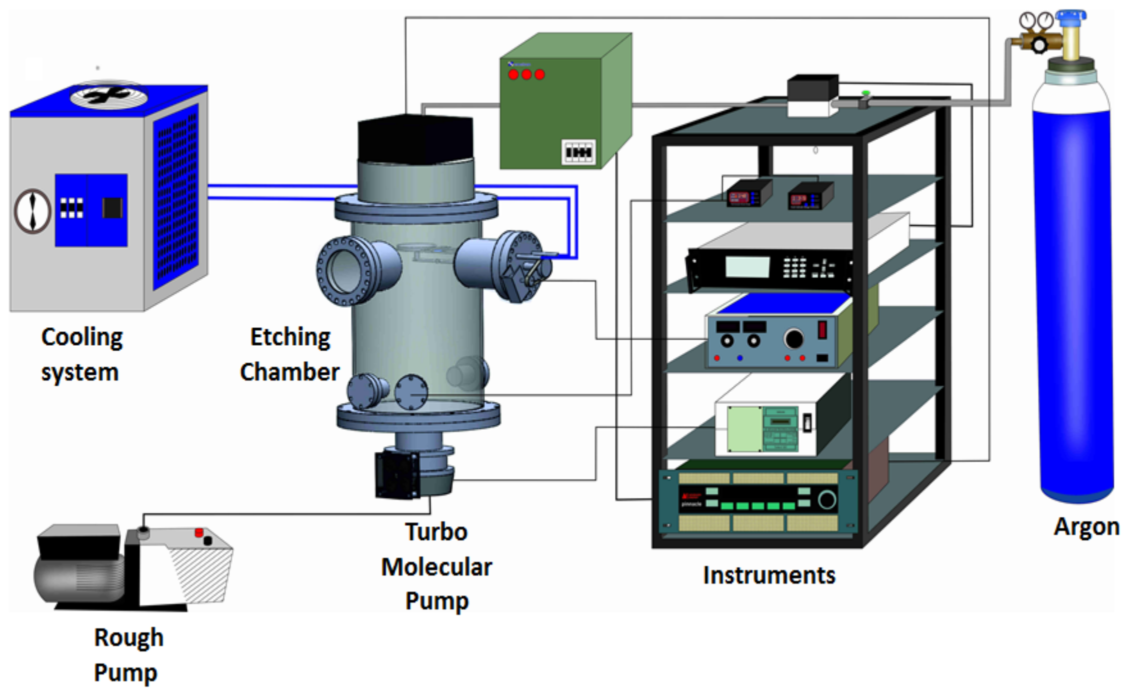

Figure 3.6. Schematic image of ion beam etching system

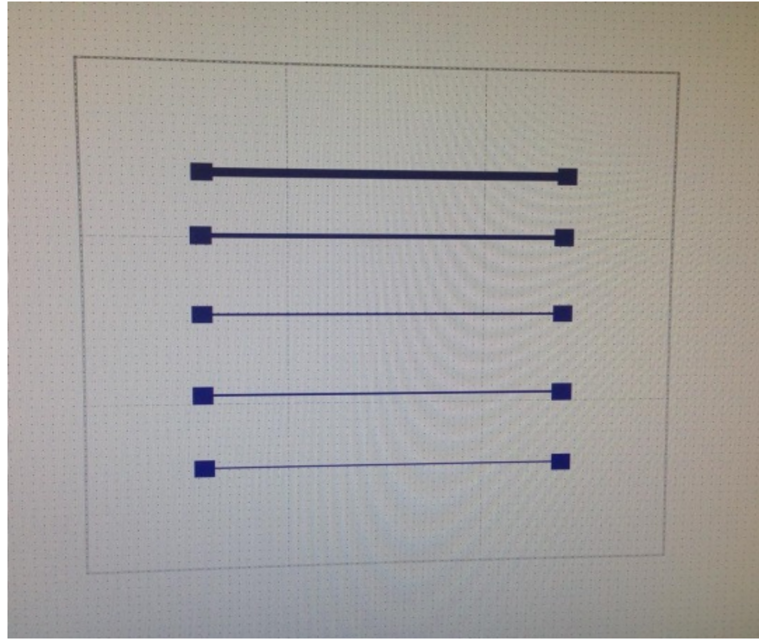

Figure 3.7. VO_2 strips with various widths

CHAPTER 4

RESULTS AND DISCUSSIONS

4.1. Scanning Electron Microscopy (SEM) Morphological Analysis

Surface morphologies of two different VO_2 thin films which were grown at 2.00 % oxygen rate with 310 nm thickness and 2.25 % oxygen rate with 125 nm thickness were investigated using scanning electron microscopy (SEM) (Figure 4.1). SEM images of these films have high magnification of 1200x. To fabricate homogeneous VO_2 phase is quietly difficult because there are important factors to obtain VO_2 phase. These important factors are substrate temperature, deposition pressure, oxygen concentration and the thickness of grown thin films. Especially, the temperature should be the same at each point on the substrate. If there is small oxygen ratio difference, or temperature difference for grown thin film, observable some differences depend on the thickness take places on the substrate.

As shown in Figure 4.2a, 310 nm VO_2 film with 2.00 % oxygen concentration has small grains. However, Figure 4.2b shows that 125 nm grown VO_2 film with 2.25 % oxygen concentration has meander like structure. The results indicate that the image of small grains transform to meander like oxygen rich grains due to increasing oxygen ratio. Moreover, increasing film thickness trigger the mechanism that provides meander like structure to small grains. This effect can be expressed with the diffusion and the migration of the adsorbed atoms. Increasing deposition time causes to diffuse and migrate on the substrate surface that is important process for nucleation and film growth (Yuce et al. 2015).

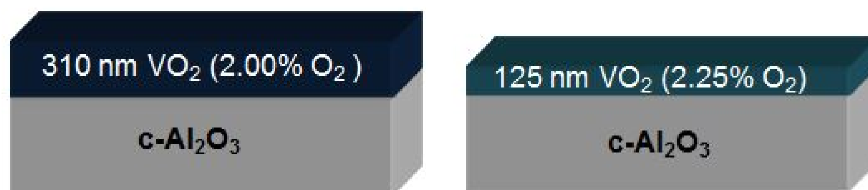

Figure 4.1. Schematic representation of VO_2 thin films on c-cut sapphire substrate with different thickness and oxygen concentration

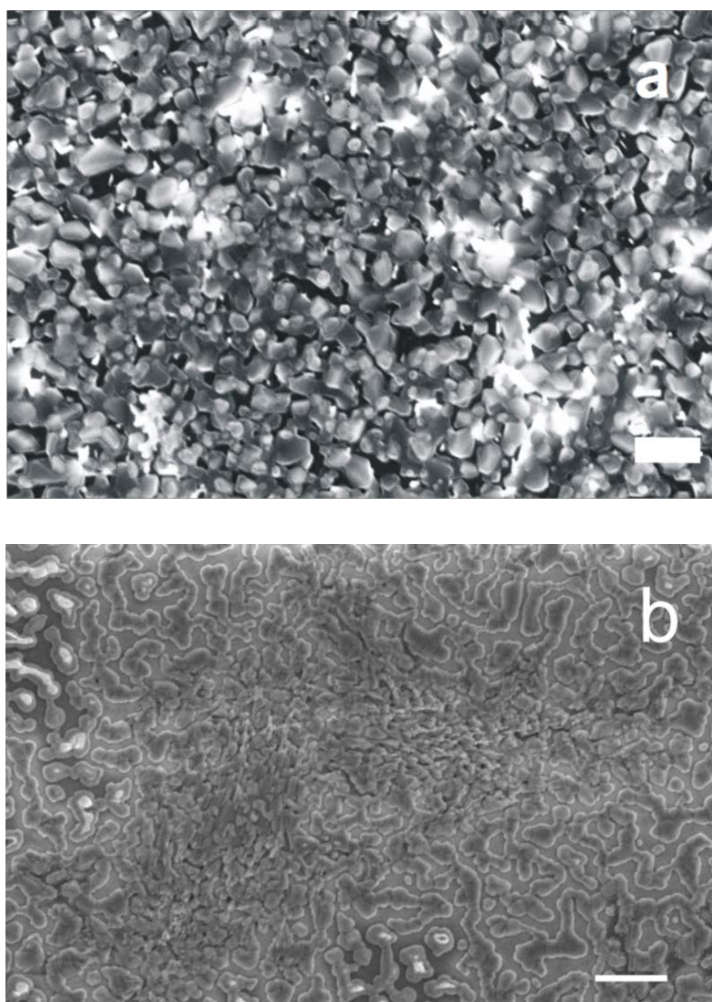

Figure 4.2. FE-SEM images of (a) 310 nm VO_2 thin film with 2.00 % oxygen ratio (b) 125 nm VO_2 thin film with 2.25 % oxygen ratio

4.2. X-Ray Diffraction (XRD) Analysis

Figure 4.3 indicates XRD analysis results of 310 nm VO_2 thin films at 2.00 % O_2 rate. In this figure, one strong diffraction ($2\Theta=29.4^{\circ}$) peak that matches to plane (011) of VO_2 was observed (Zhao et al. 2012). In addition, the spectrum shows at

angles of 36˚, 39.5˚ and 43.3˚ which are related to the reflections respectively from planes (200), (020) and (210) of VO_2 (Kim et al. 2014). According to these analyses, the peaks which have low intensity belong to V_2O_3, V_2O_5 and V_6O_{13} secondary phases (Luo et al. 2013). The intensity of V_6O_{13} is higher than the intensities of other secondary phases as shown in this figure. Consequently, although this grown VO_2 thin film seems inhomogeneous, the film exhibits VO_2 properties as near-perfect owing to its strong peak at angles 2Θ=29.4˚. This result is supported by electrical results.

When deposition time was decreased, it could not be obtained a high quality film for VO_2 phase at 2.00 % O_2 rate with the thickness of 125 nm. It is shown in Raman and optical analysis results. The best result among 125 nm grown thin films was obtained for 2.25 % O_2 rate. The XRD analysis result of this obtained VO_2 is shown in Figure 4.4. As considering this result, there is a strong peak at 2Θ=41.6˚ correspond to (0006) plane from sapphire (Al_2O_3) substrate (Zhao et al. 2012) due to the fact that this grown film is too thin to take data from only surface. The intensity of the peak comes from the substrate depend on the thickness of the film. In addition to the peak originated from the substrate, the spectrum exhibits the peaks at 2Θ=37.5˚ and 2Θ=39.8˚ which belong to the reflections from planes respectively (200) and (020) of VO_2; the peak 26.8˚ which is related to V_2O_5 secondary phase (Kim et al. 2014).

As a result, the strong peak at 29.4˚ belong to VO_2 vanished in Figure 4.4 compared to Figure 4.3. Even if there is the peak belong to V_2O_5 at low intensity without main VO_2 peak for 125 nm VO_2 thin film with 2.25 % oxygen concentration, this cause to disappear some properties of VO_2.

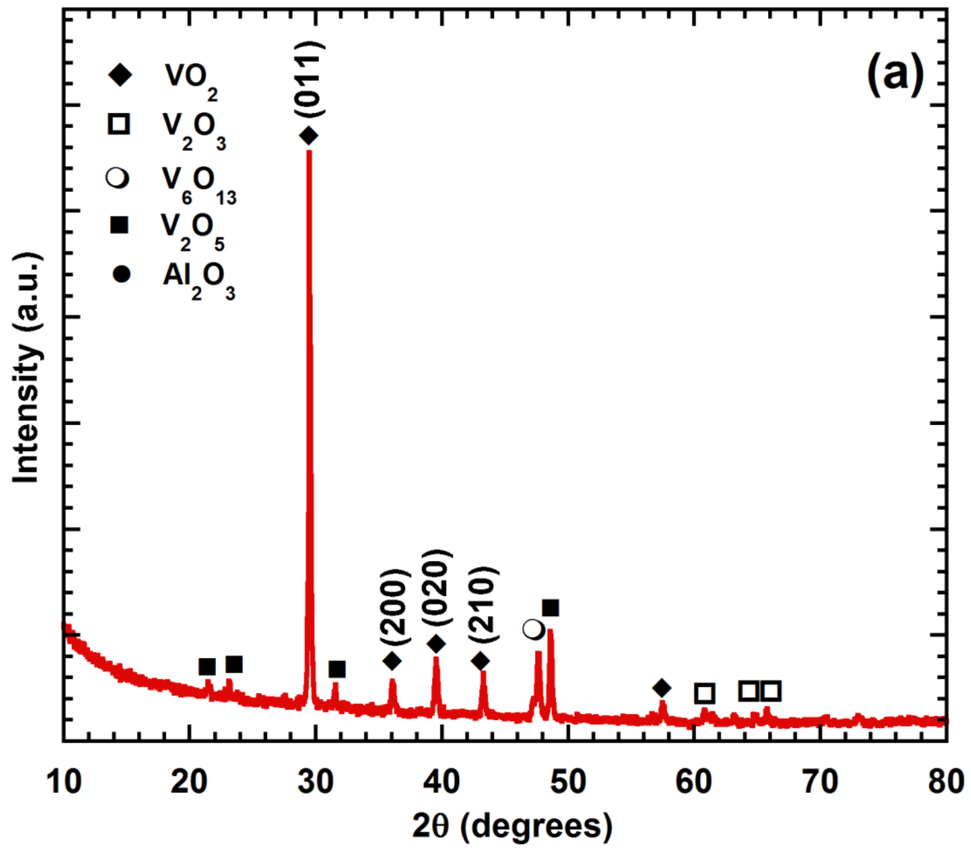

Figure 4.3. XRD pattern of 310 nm VO_2 thin film with 2.00 % oxygen ratio

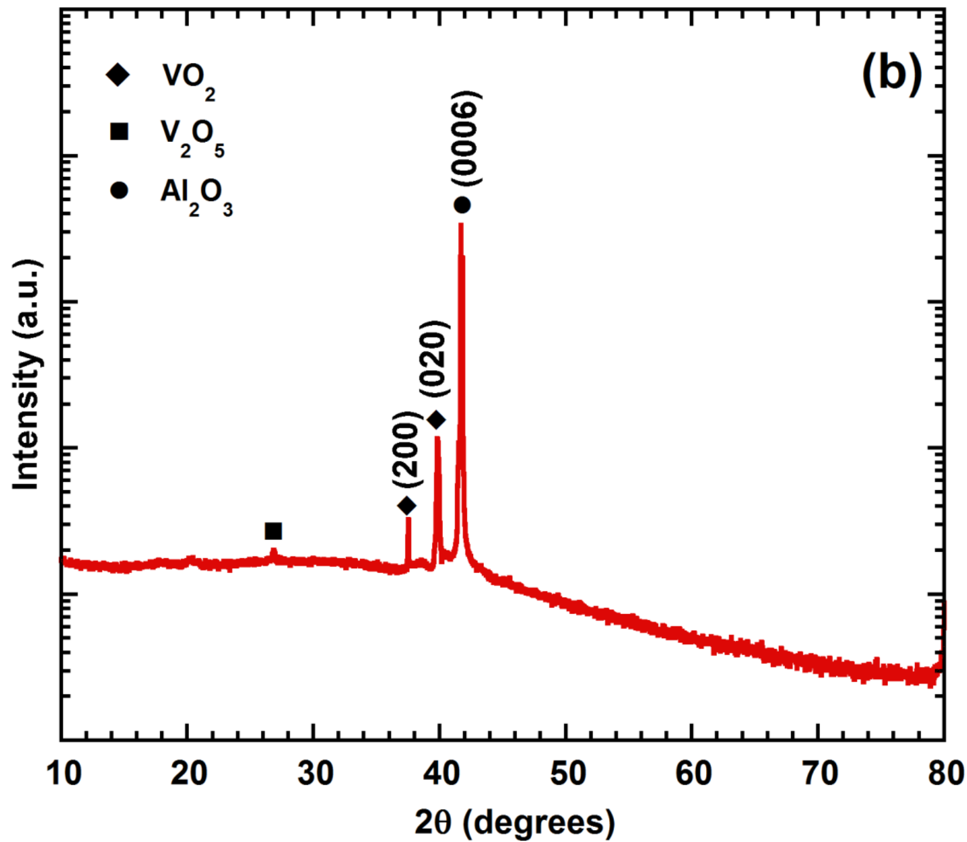

Figure 4.4. XRD pattern of 125 nm VO_2 thin film with 2.25 % oxygen ratio

4.3. Raman Analysis

In order to obtain more information about the structure of grown thin films, Raman spectra of grown VO_2 thin films were obtained at room temperature shown in Figure 4.5. As shown in this figure, In order to create VO_2 phase, they are important parameters which are not only substrate temperature during deposition but oxygen ratio and the thickness of grown films.

As regards VO_2 phase, the best Raman analysis result was observed for the grown 310 nm VO_2 films with 2.00 % oxygen ratio. The Raman modes which are 313, 342, 392, 445, 502 and 617 cm^{-1} belong to VO_2 vibration modes (Zhao et al. 2012). The peak which is at 617 cm^{-1} is the main peak of VO_2 phase and related to V-V vibration mode (Zhao et al. 2012). The deposited VO_2 films with 310 nm - 2.00 % O_2 rate and 125 nm - 2.25 % O_2 rate has strong peak at 617 cm^{-1} compared to the other films. However, the thickness of grown films decreases induces the other peaks which are at 288, 408, 488, 530, 704 and 997 cm^{-1} belong to V_2O_5 secondary phase (Piccirillo,

Binions, and Parkin 2007). As oxygen ratio of 125 nm grown vanadium decreases to 2.25 % from 3.00 %, the intensities of V_2O_5 characteristic peaks decrease, and the intensities of VO_2 characteristic peaks increase. In addition, while 310 nm VO_2 thin film at 2.00 % O_2 rate shows near-perfect results, the main peak which is at 617 cm^{-1} and several peaks correspond to VO_2 and V_2O_5 phases vanishes for 125 nm grown VO_2 thin films at the same O_2 rate. As different from other analysis results, observed Raman modes at nearly 320 and 330 cm^{-1} belong to respectively V_2O_5 and VO_2 phases (Öksüzoğlu et al. 2013, Petrov, Yakovlev, and Squier 2002). As a result, Raman analysis results confirm that the better crystallinity is obtained with increasing thickness of the grown film. Also, the best O_2 rate is 2.00 % for 310 nm and 2.25 % for 125 nm VO_2 thin film.

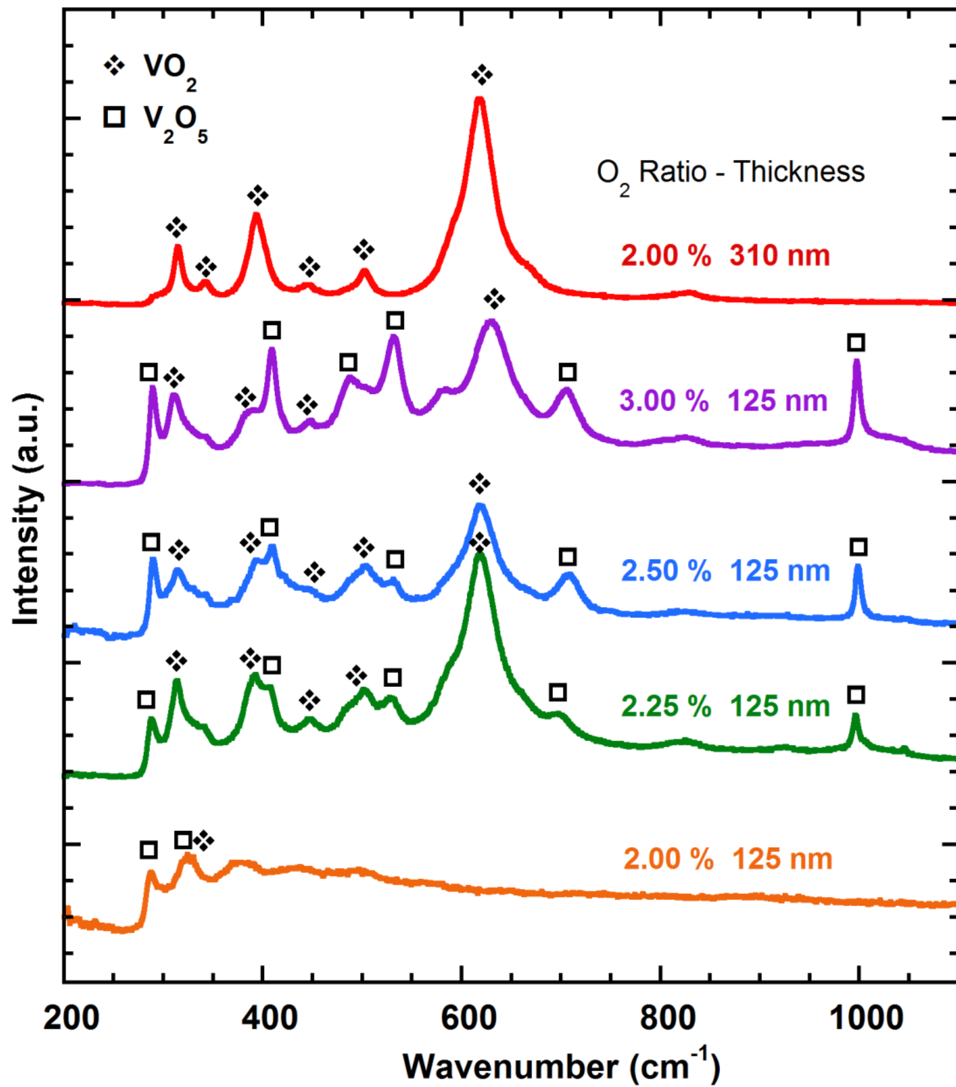

Figure 4.5. Raman spectra of grown VO_2 thin films with the thickness of 125 and 310 nm at various oxygen ratio

4.4. Optical Properties

While VO_2 thin films which is insulator material has high transmittance in near infrared region (NIR) at room temperature, VO_2 with metallic structure is opaque to infrared light at higher temperature than its transition temperature (Jiang et al. 2014).

Figure 4.6 shows the transmittance spectra between 200-2600 nm of 310 nm grown VO_2 thin film on sapphire substrate with 2.00 % oxygen ratio at room temperature and 80 ^oC. While the transmission of this thin film is around 63 % in near infrared region (NIR) at room temperature, this value becomes nearly 2 % at higher temperature than transition temperature. Due to its high thickness, the thin film has

lower transmittance in visible region. Therefore, even if the change in transmission is about 60.0 % for near-IR region, in order to obtain high transmittance in all regions at room temperature, the optical analysis of thinner films at different O_2 rate was carried out.

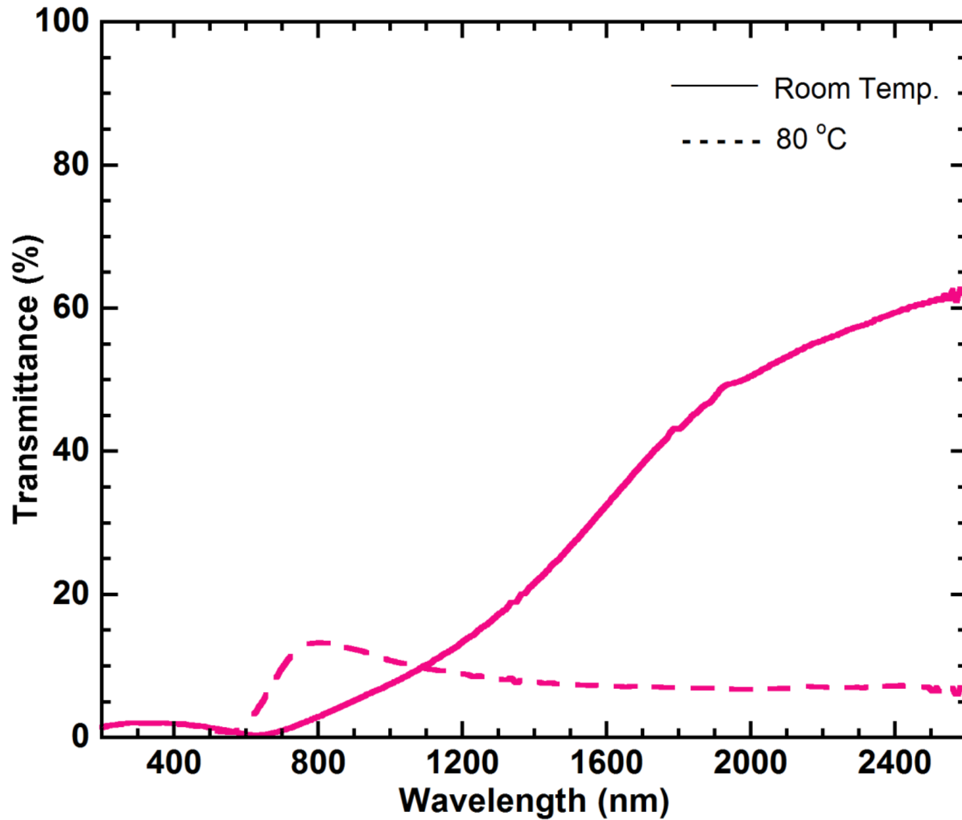

Figure 4.6. Transmittance spectra of 310 nm grown VO_2 thin film with 2.00 % oxygen ratio at room temperature and 80 ^oC

At room temperature and 80 ^oC between 200-2600 nm taken transmittance spectra of 125 nm VO_2 thin films which were deposited on sapphire substrates with different oxygen ratio are shown in Figure 4.7. Oxygen ratio between 3.00 % and 2.00 % substantially influences transmission results. The best expected transmission result among these thin films was observed at grown VO_2 thin film at 2.25 % oxygen rate in the event of comparing the transmission result of VO_2 thin film. The transmittance of grown VO_2 thin film with 2.25 % oxygen ratio decreases by nearly 40 % in NIR upon heating to 80 ^oC. The change in transmittance of grown VO_2 thin films at 3.00 % and 2.50 % O_2 rate is respectively around 10 % and 15 %. When approaching optimum oxygen ratio, the change in transmittance in NIR increases as depending on the

temperature. The percentage change in infrared transmittance could detect included VO_2 phase quantity in these deposited thin films. Because there is no change in infrared transmittance of deposited VO_2 thin film with 2.00 % oxygen ratio at any temperature, this film does not include almost VO_2 phase. Thus, optimum oxygen ratio is 2.25 % among 125 nm grown thin films with different oxygen percentage, which is supported by optical analysis results.

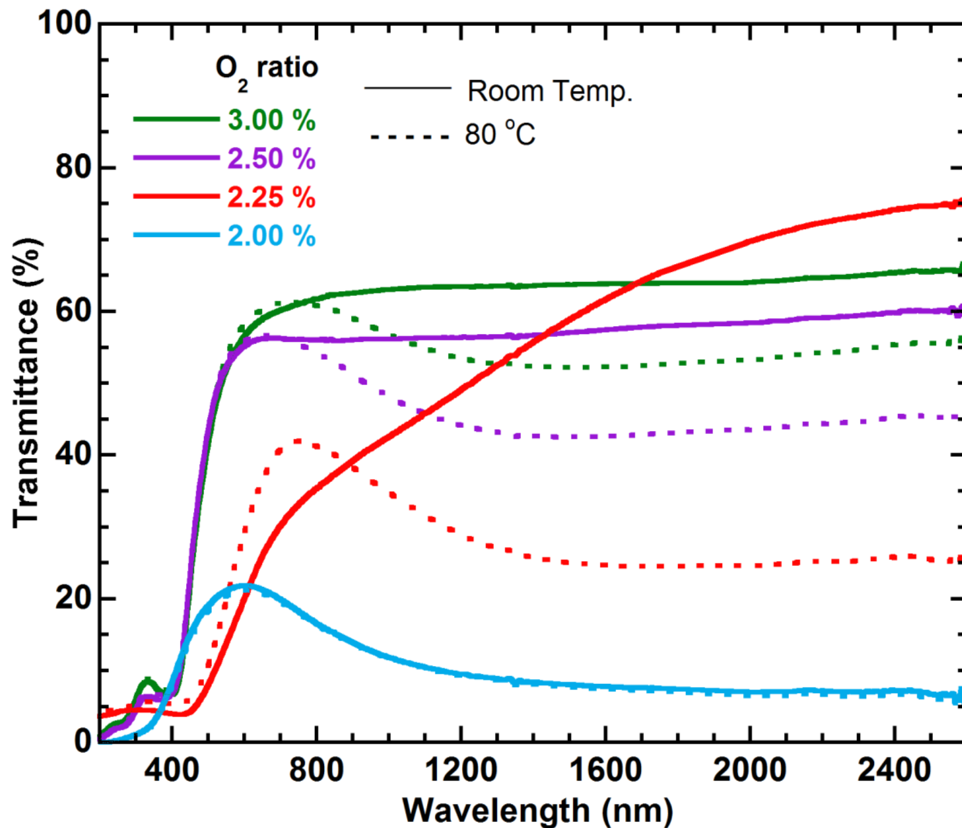

Figure 4.7. Transmittance spectra of 125 nm grown VO_2 thin films with various oxygen ratio at room temperature and 80 ^{o}C

Optical analysis results of 125 nm grown VO_2 thin film with 2.25 % oxygen ratio depends on the constant wavelength which are 550 (visible), 1600 (NIR) and 2500 nm (NIR) at different temperature are shown in Figure 4.8. The change in the transmittance percentage switches according to the wavelength of the light, and abruptly decreases at transition temperature. There is no any variation in the transmittance under 550 nm wavelengths light. However, the change in transmittance percentage for 1600 and 2500 nm is respectively 30 % and 40 %. As a result, the material has higher

transmittance depends on the being exposed region visible to near-IR with increasing the wavelength of the light.

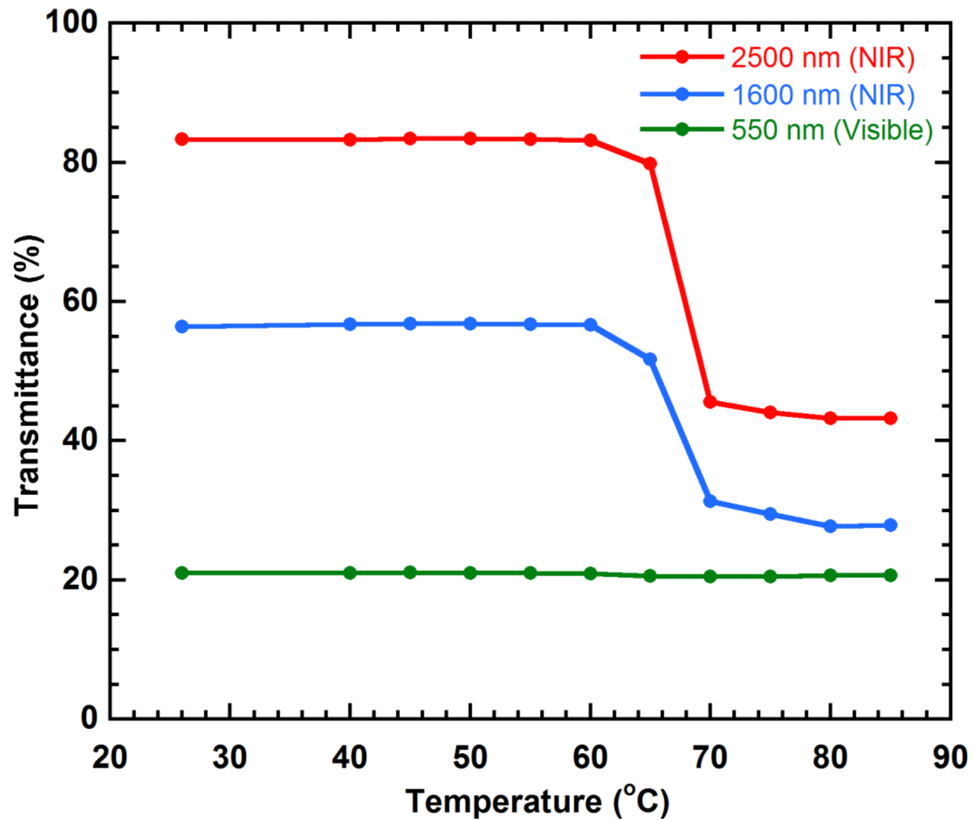

Figure 4.8. Optical switching property depends on the temperature of 125 nm VO_2 thin film with 2.25 % oxygen ratio as different wavelength

4.5. X-Ray Photoelectron Spectroscopy (XPS) Analysis

Among grown VO_2 thin films, 310 nm VO_2 film with 2.00 % O_2 ratio which gives the best results was analyzed by X-ray Photoelectron Spectroscopy (XPS) in order to determine different oxidation states on the surface of the film. The binding energy of the V $2p_{3/2}$ core level is related to the oxidation state of vanadium cation, so different vanadium cation oxidation states in vanadium oxide compounds can be determined with using curve fitting of V $2p_{3/2}$ XPS signal.

In this measurement, It is focused C 1s, O 1s, V $2p_{1/2}$ and V $2p_{3/2}$ binding energy positions. XPS spectra were taken with C 1s correction at 284.6 eV. After Shirley background addition, the sub-peaks which taken measurements were fitted as using Gaussian-Lorentzian curve fitting. In the course of XPS analysis, X-ray satellite peak

which was observed at around 520 eV binding energy and belongs to O 1s peak was disregarded. Figure 4.9 shows XPS analysis of C 1s valence band. The binding energy of C=C bond is observed at 284.6 eV. Additionally, the binding energy of C-O bond is 286.2 eV, and the binding energy of C=O bond is observed at 288.6 eV (Mortazavi et al. 2013). After that, XPS analysis was carried out for O 1s and V 2p area. It is obtained two different peaks which have different binding energies for O 1s. The peak which is observed at 530.2 eV corresponds to the bond between vanadium-oxygen (V-O). In addition, the peak at 531.3 eV belongs to the bond between carbon-oxygen (C-O). The assignment of the bond between oxygen and carbon is compatible with the analysis of O 1s and C 1s. There are two different vanadium oxide phases in the analysis of V 2p valence band. Due to spin-orbit separations, V $2p_{3/2}$ and V $2p_{1/2}$ were observed with 7.3 eV binding energy difference. Figure 4.10 shows that the binding energies at 516.2 and 517.5 eV refer to respectively VO_2 and V_6O_{13} of vanadium oxide component (Silversmit et al. 2004).

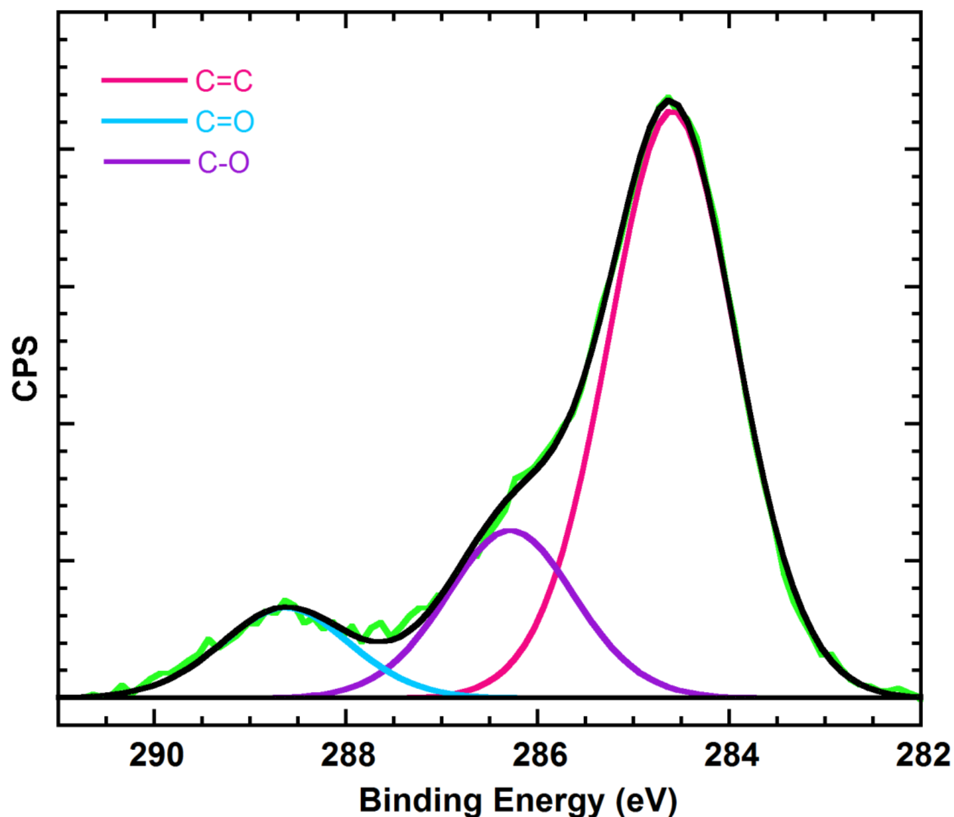

Figure 4.9. XPS analysis of carbon (C)

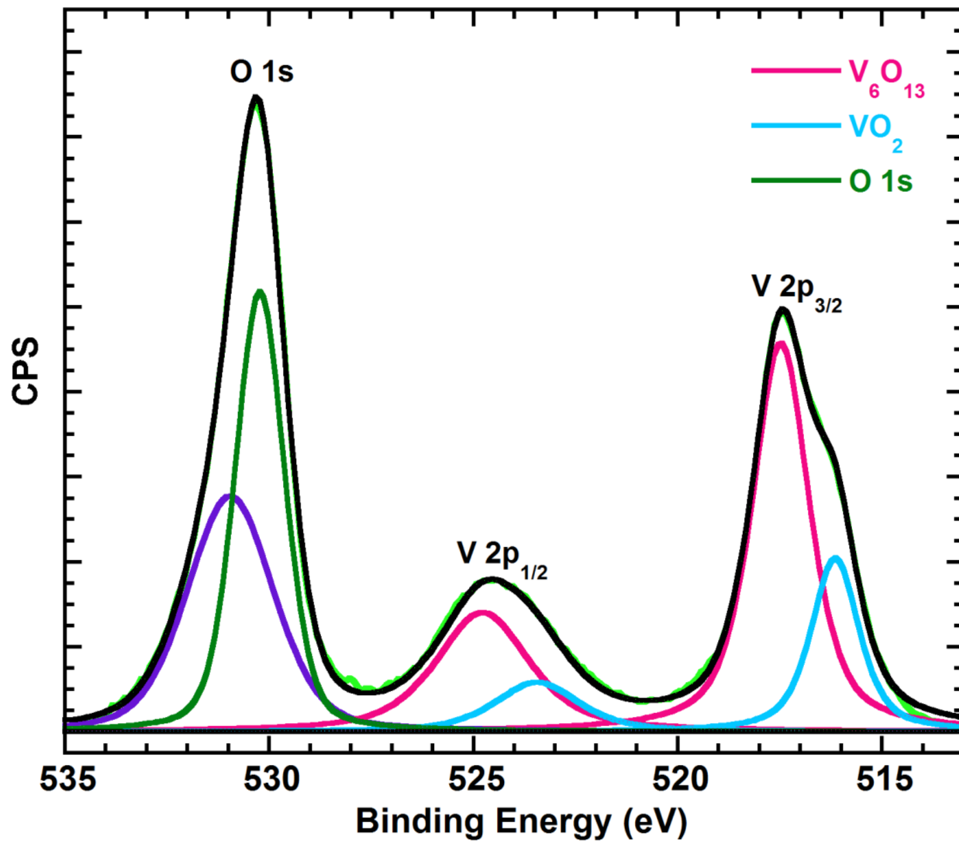

Figure 4.10. XPS analysis of 310 nm VO_2 thin film with 2.00 % oxygen ratio

4.6. Electrical Properties

Deposited VO_2 thin films indicate MIT at nearly 70 ˚C as shown in Figure 4.11. While the resistivity of 310 nm grown VO_2 (2.00 % O_2) is around 3.00 Ω.cm at room temperature, this value abruptly decreases up to $2.0x10^{-4}$ Ω.cm at higher temperature than transition temperature. The change in resistivity of 310 nm VO_2 thin film between at room temperature and 100 ˚C is nearly by a factor of 10^4. This quantity is one of the best results among reported values (Ruzmetov et al. 2010).

The resistivity of 125 nm grown VO_2 (2.25 % O_2) is nearly $1.5x10^2$ Ω.cm at room temperature. In the event of the fact that it is considered abundant VO_2 and small V_2O_5 secondary phase coexisted. According to Raman and XRD analysis results of 125 nm VO_2 (2.25 % O_2), the reason of obtained higher resistivity can be explained compared to the 310 nm VO_2 thin film. Another material affects the resistivity of VO_2 at room temperature. Whereas coexisted insulator material cause to increase the resistivity of VO_2, coexisted metallic material cause decrease the resistivity value at

room temperature. Therefore, insulator V_2O_5 leads to increase the resistivity of 125 nm VO_2 (2.25 % O_2) thin film with its high resistivity value. In addition, the resistivity of this thin film decreases up to 6.7×10^{-1} Ω.cm at high temperature compared to the transition temperature. Due to insulator V_2O_5 secondary phase, the resistivity of the thin film cannot decrease as from specific value, and insulator V_2O_5 quantity limits this value.

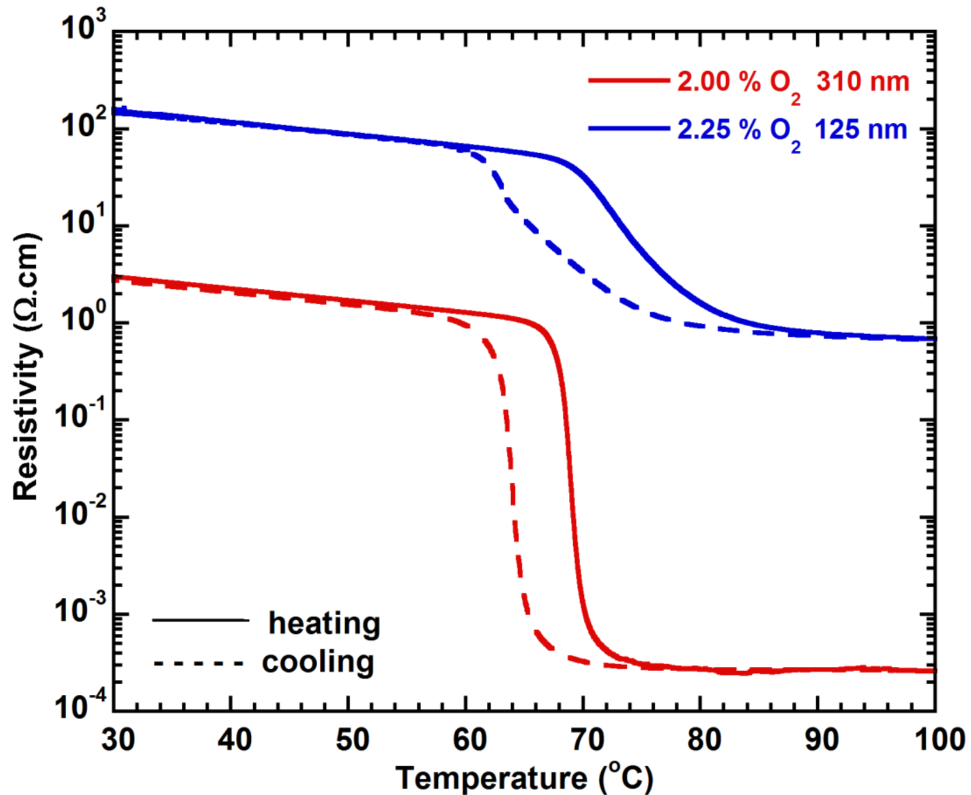

Figure 4.11. The resistivity depends on the temperature for 310 nm VO_2 thin film with 2.00 % oxygen ratio and 125 nm VO_2 thin films with 2.25 % oxygen ratio

Among grown vanadium oxide thin films, VO_2 thin film which indicated the highest change in resistivity depends on the temperature was patterned by e-beam lithography with different strips. After taken electrical measurement on silver electrodes for 4 mm x 4 mm square VO_2 sample, the resistivity of each VO_2 strip was measured at different temperatures as shown in Figure 4.12. The widths of the strips of VO_2 square sample are 50, 20, 15 and 10 μm. After electron beam lithography process, the resistivity of VO_2 strips decreased down to around 10^{-2} Ω.cm at room temperature. The reason of this situation may be the deterioration in VO_2 chemical structure under high

voltage during electron beam process. Therefore, the change in resistivity of VO_2 strips is around by an order of one. In addition, this process leaded to the shift of transition temperature to nearly 50 ˚C.

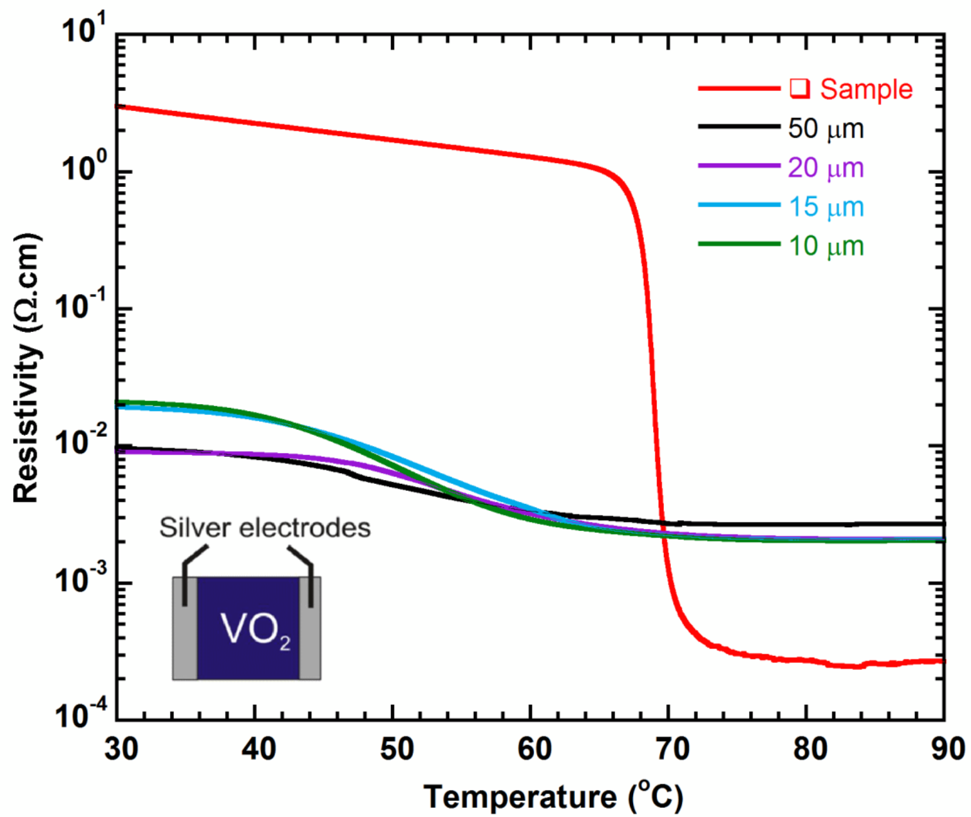

Figure 4.12. The resistivity depends on the temperature for shaped 310 nm VO_2 thin film at 2.00 % oxygen ratio.

CHAPTER 5

CONCLUSION

Vanadium dioxide (VO_2) exhibits metal-insulator transition (MIT) at 70 ˚C. At the MIT temperature, electrical and optical properties of VO_2 changes with its crystal structure. VO_2 has high potential for electronic devices among vanadium oxide (VO_x) compounds because the transition temperature of VO_2 is closer to room temperature compared to the other VO_x compounds.

For thin film fabrication, we used DC sputtering technique which is highly attractive due to its controllability and strong adhesion. Additionally, the other advantage is good thickness uniformity which is essential for thin film production.

We worked on VO_2 thin film fabrication. As the first step, magnetron sputtering system was designed with a heater system, and to provide homogeneity a rotation mechanism was employed. In order to grow thin film, optimum system conditions were determined. To obtain VO_2 single phase, ideal growth parameters were investigated. The effects of oxygen concentration and thickness on grown thin films were examined. VO_2 thin films were deposited on c-sapphire at various oxygen rates with different film thickness. Optical and Raman analysis results show that oxygen concentration in the film could change with the thickness of the thin film. 310 nm VO_2 thin film with 2.00 % oxygen ratio has nearly 60.0 % change in transmission as depending temperature at near-IR region. However, for visible region, this change in transmittance is quite low due to the thickness of the film. When film thickness reduces to 125 nm, there is no change in transmission at the same oxygen concentration. Then, oxygen ratio was increased up to 3.00 % from 2.00 % for 125 nm VO_2 thin films. According to optical analysis results, no change in transmittance of 125 nm VO_2 thin film (2.00 % O_2) was not observed while the change in transmittance of 125 nm VO_2 thin film (2.25 % O_2) is nearly 50.0 % at near-IR region. We can say that not only thickness but oxygen concentration is important parameter in fabrication of VO_2 thin film. In the event of decreasing thickness of the VO_2 film, oxygen concentration in the film may decrease and the film acquires metallic property. Therefore, due to crystallization, when film thickness is decreased, the enhancement of O_2 ratio in the film may be necessary.

Additionally, our findings were supported by Raman analysis. That is, for 310 nm VO_2 thin film (2.00 % O_2 ratio), only VO_2 Raman modes were observed with high intensity, but for 125 nm VO_2 thin film (2.00 % O_2 ratio) it was observed that only one peak belong to VO_2 Raman mode with low intensity. According to optical and Raman analysis results 125 nm VO_2 thin film with 2.25 % ratio gives the best result among thinner films. For 125 nm VO_2 with 2.00 % oxygen concentration, the film was observed as metallic, but the others include V_2O_5 secondary phase.

For 310 nm VO_2 (2.00 % O_2) thin film, MIT was observed at 70 ˚C with temperature dependence change in resistivity by a factor 10^4. This factor is the highest value in the literature for magnetron sputtered VO_2. Utilizing this resistivity change, fabricated VO_2 is available for a lot of applications such as logic circuits, detectors or thermochromic windows. Additionally, for 125 nm VO_2 (2.25 % O_2) thin film, the change in resistivity was an order of 2 because this film includes both VO_2 and V_2O_5 phases. Due to V_2O_5 which is an insulator at the range of measured temperature, High resistivity change was not observed.

For field effect transistor (FET) applications, VO_2 channel was fabricated. VO_2 thin square film (4mm x 4mm) was patterned into strips with various widths by electron beam lithography. During patterning steps, VO_2 strips were exposed to high voltage and were chemically processed. Therefore, these VO_2 strips produced different results compared to square VO_2 sample. After electron beam process, at room temperature the resistivity of VO_2 strips decreased down to around 10^{-2} Ω.cm from 3.0 Ω.cm. The change in the resistivity of these strips is at around by an order of one. Moreover, for VO_2 strips, it was observed that transition temperature shifted to 50 ˚C. The transition temperature is closer to room temperature, which means an increased efficiency for thermochromic window applications.

REFERENCES

Atkin, Joanna M, Samuel Berweger, Emily K Chavez, Markus B Raschke, Jinbo Cao, Wen Fan, and Junqiao Wu. 2012. "Strain and temperature dependence of the insulating phases of VO_2 near the metal-insulator transition." *Physical Review B* 85 (2):020101.

Basov, Dimitri N, Richard D Averitt, Dirk Van Der Marel, Martin Dressel, and Kristjan Haule. 2011. "Electrodynamics of correlated electron materials." *Reviews of Modern Physics* 83 (2):471.

Belyaev, MA, AA Velichko, PP Boriskov, NA Kuldin, VV Putrolaynen, and GB Stefanovitch. 2014. "The Field Effect and Mott Transistor Based on Vanadium Dioxide."

Brinkman, WF, and TM Rice. 1970. "Application of Gutzwiller's variational method to the metal-insulator transition." *Physical Review B* 2 (10):4302.

Chae, BG, DH Youn, HT Kim, SY Maeng, and KY Kang. 2003. "Fabrication and electrical properties of pure VO_2 phase films." *arXiv preprint cond-mat/0311616*.

Chae, Byung Gyu, Hyun Tak Kim, and Sun Jin Yun. 2008. "Characteristics of W-and Ti-doped VO_2 thin films prepared by sol-gel method." *Electrochemical and Solid-State Letters* 11 (6):D53-D55.

Chen, Changhong, Xinjian Yi, Xingrong Zhao, and Bifeng Xiong. 2001. "Characterizations of VO2-based uncooled microbolometer linear array." *Sensors and Actuators A: Physical* 90 (3):212-214.

Demirhan, Yasemin. 2014. "Fabrication of double mesa structures from superconducting Bi2Sr2CaCu2O8+ d by e-beam lithography for terahertz emission." İzmir Institute of Technology.

Du, Jing, Yanfeng Gao, Hongjie Luo, Litao Kang, Zongtao Zhang, Zhang Chen, and Chuanxiang Cao. 2011. "Significant changes in phase-transition hysteresis for Ti-doped VO_2 films prepared by polymer-assisted deposition." *Solar Energy Materials and Solar Cells* 95 (2):469-475.

Eguchi, Ritsuko, Takayoshi Yokoya, Takayuki Kiss, Yutaka Ueda, Hiroyuki Tajima, Jun Yamazaki, and Shik Shin. 2002. "Angle-resolved photoemission spectroscopy, optical conductivity, and soft X-ray Raman spectroscopy of quasi-one-dimensional V_6O_{13}." *Physica B: Condensed Matter* 312:600-602.

Filonenko, VP, M Sundberg, P-E Werner, and IP Zibrov. 2004. "Structure of a high-pressure phase of vanadium pentoxide, β-V_2O_5." *Acta Crystallographica Section B: Structural Science* 60 (4):375-381.

Gebhard, Florian. 1997. *Metal—Insulator Transitions*: Springer.

Gopalakrishnan, Gokul, Dmitry Ruzmetov, and Shriram Ramanathan. 2009. "On the triggering mechanism for the metal–insulator transition in thin film VO_2 devices: electric field versus thermal effects." *Journal of materials science* 44 (19):5345-5353.

Gottimukkala, Roja. 2005. "Growth and characterization of diamond and diamond like carbon films with interlayer."

Griffiths, Peter R, and James A De Haseth. 2007. *Fourier transform infrared spectrometry*. Vol. 171: John Wiley & Sons.

Gu, Yijia, Jinbo Cao, Junqiao Wu, and Long-Qing Chen. 2010. "Thermodynamics of strained vanadium dioxide single crystals." *Journal of Applied Physics* 108 (8):083517.

Hood, PJ, and JF DeNatale. 1991. "Millimeter-wave dielectric properties of epitaxial vanadium dioxide thin films." *Journal of applied physics* 70 (1):376-381.

Imada, Masatoshi, Atsushi Fujimori, and Yoshinori Tokura. 1998. "Metal-insulator transitions." *Reviews of Modern Physics* 70 (4):1039.

Jiang, Meng, Xun Cao, Shanhu Bao, Huaijuan Zhou, and Ping Jin. 2014. "Regulation of the phase transition temperature of VO_2 thin films deposited by reactive magnetron sputtering without doping." *Thin Solid Films* 562:314-318.

Johansson, Daniel. 2006. "VO_2 films as active infrared shutters."

Jordan, Tyler S, Simon Scott, Darin Leonhardt, Joyce Olsen Custer, Christopher T Rodenbeck, Steve Wolfley, and Christopher D Nordquist. 2014. "Model and Characterization of Thin-Film Switching Devices." *Electron Devices, IEEE Transactions on* 61 (3):813-819.

Kim, DH, and HS Kwok. 1994. "Pulsed laser deposition of VO_2 thin films." *Applied physics letters* 65 (25):3188-3190.

Kim, H, N Charipar, M Osofsky, SB Qadri, and A Piqué. 2014. "Optimization of the semiconductor-metal transition in VO_2 epitaxial thin films as a function of oxygen growth pressure." *Applied Physics Letters* 104 (8):081913.

Kim, Hyun-Tak. 2002. "New trends in superconductivity." *NATO science series* 2:67.

Kim, Hyun-Tak, Byung-Gyu Chae, Doo-Hyeb Youn, Sung-Lyul Maeng, Gyungock Kim, Kwang-Yong Kang, and Yong-Sik Lim. 2004. "Mechanism and observation of Mott transition in VO2-based two-and three-terminal devices." *New Journal of Physics* 6 (1):52.

Klug, Harold Philip, and Leroy Elbert Alexander. 1954. "X-ray diffraction procedures."

Ko, Changhyun, and Shriram Ramanathan. 2008. "Stability of electrical switching properties in vanadium dioxide thin films under multiple thermal cycles across the phase transition boundary." *Journal of Applied Physics* 104 (8):6105.

Kumar, RT Rajendra, B Karunagaran, D Mangalaraj, Sa K Narayandass, P Manoravi, M Joseph, Vishnu Gopal, RK Madaria, and JP Singh. 2003. "Room temperature deposited vanadium oxide thin films for uncooled infrared detectors." *Materials research bulletin* 38 (7):1235-1240.

Lieberman, Michael A, and Allan J Lichtenberg. 1994. "Principles of plasma discharges and materials processing." *MRS Bulletin* 30:899-901.

Liu, Kai, Chun Cheng, Joonki Suh, Robert Tang-Kong, Deyi Fu, Sangwook Lee, Jian Zhou, Leon O Chua, and Junqiao Wu. 2014. "Powerful, Multifunctional Torsional Micromuscles Activated by Phase Transition." *Advanced Materials* 26 (11):1746-1750.

Luo, YY, LQ Zhu, YX Zhang, SS Pan, SC Xu, M Liu, and GH Li. 2013. "Optimization of microstructure and optical properties of VO_2 thin film prepared by reactive sputtering." *Journal of Applied Physics* 113 (18):183520.

Marezio, M, Do B McWhan, JP Remeika, and PD Dernier. 1972. "Structural Aspects of the Metal-Insulator Transitions in Cr-Doped VO_2." *Physical Review B* 5 (7):2541.

Maruyama, T, and Y Ikuta. 1993. "Vanadium dioxide thin films prepared by chemical vapour deposition from vanadium (III) acetylacetonate." *Journal of materials science* 28 (18):5073-5078.

Morin, FJ. 1959. "Oxides which show a metal-to-insulator transition at the Neel temperature." *Physical Review Letters* 3 (1):34.

Mortazavi, Seyedeh Zahra, Parviz Parvin, Ali Reyhani, Soghra Mirershadi, and Rasoul Sadighi-Bonabi. 2013. "Generation of various carbon nanostructures in water using IR/UV laser ablation." *Journal of Physics D: Applied Physics* 46 (16):165303.

Mott, Nevill. 1990. "On metal-insulator transitions." *Journal of Solid State Chemistry* 88 (1):5-7.

Mott, NF, and Metal-Insulator Transitions. 1990. "Taylor and Francis." *New York*.

Nag, Joyeeta. 2011. "The solid-solid phase transition in vanadium dioxide thin films: synthesis, physics and application." Vanderbilt University.

Nazari, Mohammad. 2013. "Vibrational and Optical Properties of Vanadium Dioxide." Texas Tech University.

Nazari, Mohammad, Changhong Chen, AA Bernussi, ZY Fan, and Mark Holtz. 2011. "Effect of free-carrier concentration on the phase transition and vibrational properties of VO_2." *Applied Physics Letters* 99 (7):071902.

Ohno, Hideo. 1998. "Making nonmagnetic semiconductors ferromagnetic." *science* 281 (5379):951-956.

Öksüzoğlu, Ramis Mustafa, Pınar Bilgiç, Mustafa Yıldırım, and Okan Deniz. 2013. "Influence of post-annealing on electrical, structural and optical properties of vanadium oxide thin films." *Optics & Laser Technology* 48:102-109.

Paterson, E, and R Swaffield. 1994. "X-ray photoelectron spectroscopy." In *Clay Mineralogy: Spectroscopic and Chemical Determinative Methods*, 226-259. Springer.

Petrov, GI, VV Yakovlev, and J Squier. 2002. "Raman microscopy analysis of phase transformation mechanisms in vanadium dioxide." *Applied physics letters* 81 (6):1023-1025.

Piccirillo, Clara, Russell Binions, and Ivan P Parkin. 2007. "Synthesis and functional properties of vanadium oxides: V_2O_3, VO_2, and V_2O_5 deposited on glass by aerosol-assisted CVD." *Chemical Vapor Deposition-Weinheim* 13 (4):145.

Ruzmetov, Dmitry, Gokul Gopalakrishnan, Jiangdong Deng, Venkatesh Narayanamurti, and Shriram Ramanathan. 2009. "Electrical triggering of metal-insulator transition in nanoscale vanadium oxide junctions." *Journal of Applied Physics* 106 (8):083702.

Ruzmetov, Dmitry, Gokul Gopalakrishnan, Changhyun Ko, Venkatesh Narayanamurti, and Shriram Ramanathan. 2010. "Three-terminal field effect devices utilizing thin film vanadium oxide as the channel layer." *Journal of Applied Physics* 107 (11):114516.

Ruzmetov, Dmitry, Kevin T Zawilski, Venkatesh Narayanamurti, and Shriram Ramanathan. 2007. "Structure-functional property relationships in rf-sputtered vanadium dioxide thin films." *Journal of Applied Physics* 102 (11):113715.

Sahana, MB, GN Subbanna, and SA Shivashankar. 2002. "Phase transformation and semiconductor-metal transition in thin films of VO_2 deposited by low-pressure metalorganic chemical vapor deposition." *Journal of applied physics* 92 (11):6495-6504.

Silversmit, Geert, Diederik Depla, Hilde Poelman, Guy B Marin, and Roger De Gryse. 2004. "Determination of the V2p XPS binding energies for different vanadium oxidation states (V^{5+} to V^{0+})." *Journal of Electron Spectroscopy and Related Phenomena* 135 (2):167-175.

Smith, Evan M, James C Ginn, Andrew P Warren, Christopher J Long, Deep Panjwani, Robert E Peale, and David J Shelton. 2014. "Linear bolometer array using a high TCR VOx-Au film." SPIE Defense+ Security.

Stefanovich, G, A Pergament, and D Stefanovich. 2000. "Electrical switching and Mott transition in VO_2." *Journal of Physics: Condensed Matter* 12 (41):8837.

Tan, Xiaogang, Tao Yao, Ran Long, Zhihu Sun, Yajuan Feng, Hao Cheng, Xun Yuan, Wenqing Zhang, Qinghua Liu, and Changzheng Wu. 2012. "Unraveling metal-insulator transition mechanism of VO2 triggered by tungsten doping." *Scientific reports* 2.

Taşdemir, Adnan. 2015. "Thin film coating of silver on fibers by roll to roll inverted cylindrical magnetron sputtering." İzmir Institute of Technology.

Tokura, Y, Y Taguchi, Y Okada, Y Fujishima, T Arima, K Kumagai, and Y Iye. 1993. "Filling dependence of electronic properties on the verge of metal–Mott-insulator transition in $Sr_{1-x}La_xTiO_3$." *Physical review letters* 70 (14):2126.

Turrell, George, and Jacques Corset. 1996. *Raman microscopy: developments and applications*: Academic Press.

Venables, John. 2000. *Introduction to surface and thin film processes*: Cambridge University Press.

Wang, Bin, Jianjun Lai, Hui Li, Haoming Hu, and Sihai Chen. 2013. "Nanostructured vanadium oxide thin film with high TCR at room temperature for microbolometer." *Infrared Physics & Technology* 57:8-13.

Wasa, Kiyotaka, Makoto Kitabatake, and Hideaki Adachi. 2004. *Thin film materials technology: sputtering of control compound materials*: Springer Science & Business Media.

West, Kevin G, Jiwei Lu, Jiani Yu, David Kirkwood, Wei Chen, Yonghang Pei, John Claassen, and Stuart A Wolf. 2008. "Growth and characterization of vanadium dioxide thin films prepared by reactive-biased target ion beam deposition." *Journal of Vacuum Science and Technology. A, International Journal Devoted to Vacuum, Surfaces, and Films* 26 (1).

Wu, Changzheng, Feng Feng, and Yi Xie. 2013. "Design of vanadium oxide structures with controllable electrical properties for energy applications." *Chemical Society Reviews* 42 (12):5157-5183.

Wu, Jyh Ming, and Lian Bang Liou. 2011. "Room temperature photo-induced phase transitions of VO_2 nanodevices." *Journal of Materials Chemistry* 21 (14):5499-5504.

Yuce, Hurriyet, Hakan Alaboz, Yasemin Demirhan, Mehtap Ozdemir, Lutfi Ozyuzer, Gulnur Aygun. 2015. "Pattern dependent resistivity and metal-insulator transition of magnetron sputtered vanadium dioxide thin films" *Applied Surface Science* (submitted)

Zallen, Richard, and Claude M Penchina. 1986. "The physics of amorphous solids." *American Journal of Physics* 54 (9):862-863.

Zhang, XY, MJ Rozenberg, and G Kotliar. 1993. "Mott transition in the d=∞ Hubbard model at zero temperature." *Physical review letters* 70 (11):1666.

Zhao, Yong, Joon Hwan Lee, Yanhan Zhu, M Nazari, Changhong Chen, Haiyan Wang, Ayrton Bernussi, Mark Holtz, and Zhaoyang Fan. 2012. "Structural, electrical, and terahertz transmission properties of VO2 thin films grown on c-, r-, and m-plane sapphire substrates." *Journal of Applied Physics* 111 (5):053533.